STD RESEARCH CORPORATION
BOX 4127, CATALINA STATION • PASADENA, CALIFORNIA 91106
TELEPHONE: (213) 684-1771

Contract No. NAS 2-3580 STD-68-2

NOVEL METHOD FOR DETERMINATION OF ENERGY-LOSS FACTORS FOR SLOW ELECTRONS IN HOT GASES

INTERIM REPORT

Covering the period 28 April 1966-30 June 1968

Prepared for

National Aeronautics and Space Administration
Ames Research Center
Magnetoplasmadynamics Branch
(Howard Stine, Technical Monitor, Mail Station N-229-2)
Moffett Field, California 94035

1 August 1968

CONTENTS

LIST OF TABLES

LIST OF FIGURES

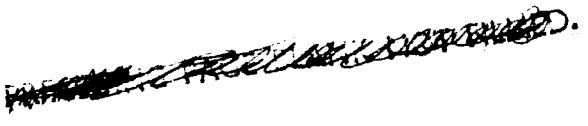

LIST OF FIGURES (Concluded)

[redacted]

LIST OF SYMBOLS

a	Width of waveguide
A_r	Cross-sectional area of waveguide
b	Height of waveguide
$\vec{B}$	Magnetic induction
d	Thickness of plasma, equation (A-3)
D_p	Diameter of Langmuir probe
e	Charge of the electron (a positive number as defined), $e_e = -e$
E	Applied (rf) electric field, $\vec{E}$ = electric field vector
E_o	Amplitude of applied (rf) electric field
ΔE_o	Experimental error in E_o, Appendix B
E_p	Characteristic plasma field, equation (31)
f	Frequency (cycles per second)
f_e	Distribution function for electrons
$(\partial f_e/\partial t)_c$	Rate of change of f_e due to collisions
f_p	Critical plasma frequency (Hz), $f_p = 9 n_e^{1/2}$
$g_{e\kappa}$	Relative speed between an electron and a molecule of species κ
$\langle g_{e\kappa} \rangle_o$	Relative speed $g_{e\kappa}$ averaged over a Maxwellian distribution
$\vec{J}_e$	Total electron current
k	Boltzmann's constant or (Appendix A) wavenumber, $2\pi/\lambda$
k_o	Wavenumber, equation (A-1) of Appendix A
m_e	Mass of the electron
m_κ	Mass of a molecule of species κ
M_f	Mole fraction of oxygen in experiments with N_2-O_2 mixtures

n_a	Neutral particle density
n_e	Number density of electrons
n_κ	Number density of species κ
p_e	Pressure of the electron gas
P	Applied rf power (equation (19) and Appendix A)
$(\Delta P)_{min}$	Minimum power required, defined following equation (29)
P_{nm}	Power transmitted in propagating mode of waveguide, equation (A-5) of Appendix A
$\vec{q}_e$	Energy flux vector for electrons, equation (1)
Q_{ea}	Collision cross-section for momentum transfer between electrons and neutral particles of species a
$Q_{e\kappa}$	Effective cross-section for momentum transfer between electrons and species κ, equation (14)
$Q_{e\kappa, s}$	Effective cross-section for energy transfer between electrons and the s degree of freedom (translational, rotational or vibrational) of species κ, equation (12)
$R_e^{(2)}$	Collisional energy exchange integral, equation (2) and equation (4)
$[R_e^{(2)}]_{el}$	Collisional energy exchange integral, elastic collisions only
$[R_e^{(2)}]_{inel}$	Collisional energy exchange integral, inelastic collisions only
R_M	Ratio defined by equation (21)
$\dot{R}$	Radiative energy loss rate (ergs/sec - cm^3)
s_i	Rate of reaction (number/sec - cm^3), equation (4)
t	Time
T	Temperature
T_e	Electron temperature; T_{e1} denotes an initial value
ΔT_e	Increment of electron temperature, $\Delta T_e = T_e - T_{e1}$
$(\Delta T_e)_{min}$	Minimum permissible change of electron temperature, equation (29)
$T_{e, E=0}$	Electron temperature with no applied electric field
T_κ	Temperature of species κ ; T_g = effective gas temperature

T_{trans}	Temperature associated with translational motion, T_{tr}
T_{rot}	Temperature of rotational degrees of freedom
T_{vib}	Temperature of vibrational degrees of freedom
T_o	Stagnation temperature
T_{elec}	Temperature of electronic degrees of freedom
$T_{\kappa, s}$	$T_{\kappa, rot}$, $T_{\kappa, vib}$, or $T_{\kappa, tr}$ (see equation (8))
T_n	Reference temperature, equation (9)
T_j^*	Excitation temperature for a class j of energy states (electronic, vibrational, rotational)
$\vec{u}_e$	Particle velocity for electrons
$\vec{U}$	Mass average velocity of gas
$\vec{w}_e$	Particle velocity (drift) relative to mass average velocity
$\vec{W}_e$	Average of $\vec{w}_e$ over velocity distribution, $\vec{W}_e = \langle \vec{w}_e \rangle$
x	Coordinate along direction of flow
X	$X = T_e - T$, Appendix B
ΔX	Experimental error in X, Appendix B
y, z	Coordinates normal to direction of flow
Z	Impedance, equations (19) and (A-7), $Z = (\mu/\epsilon)^{1/2}$
$Z_{k, n, m}$	Defined in equation (A-2)
δ	Electron energy loss factor
$\Delta\delta$	Error in δ, Appendix B
δ_κ	Energy loss factor, average fraction of energy lost per collision between an electron and a molecule of species κ
$\delta_{\kappa, el}$	Energy loss factor for elastic collisions, $\delta_{\kappa, el} = 2m_e/m_\kappa$
$\delta_{\kappa, s}$	Energy loss factor for the s class of energy states (translational, rotational or vibrational) for species κ; see equation (13)
δ_e	Energy loss factor, electron-electron collisions
δ_{eff}	Effective energy loss factor for a gas mixture $\equiv \sum_\kappa \sum_s \delta_{\kappa, s} \cdot (\tau_{e, \kappa}^{-1}/\nu_t)(T_e - T_{\kappa, s})/(T_e - T_n)$

ϵ	Quantity appearing in equation (17)
ϵ_i	Energy per reaction, equation (4)
η	$\eta = (1 - \omega_p^2/\omega^2)^{1/2}$, Appendix A
θ_v	Characteristic temperature for vibrational excitation
θ_{rot}	Characteristic temperature for rotational excitation
θ_{elec}	Characteristic temperature for electronic excitation
λ	Wavelength, Appendix A
λ_o	Debye length, equation (26)
ν_{eff}	Effective number of collisions per second for electrons
ν_{te}	Total effective collision frequency for energy transfer (electrons)
ν_t	Defined in equation (6)
$\nu_{e,\kappa}$	Collision frequency for electrons with molecules of species κ
$\nu_{e,\kappa,s}$	Defined by equation (12)
Π	Quantity appearing in equation (17)
$\overleftrightarrow{\pi}_e$	Stress tensor for electrons, $\overleftrightarrow{\pi}_e = \rho_e \langle \vec{w}_e \vec{w}_e \rangle$
ρ	Reflectivity, equation (A-3)
$\tau_{e,e}$	Effective collision time for momentum transfer among electrons
$\tau_{e,e,e}$	Effective collision time for energy transfer among electrons
$\tau_{e,\kappa}$	Effective collision time for momentum transfer between electrons and particles of species κ, $(4/3)\tau_{e,\kappa} = 1/\nu_{e,\kappa}$
$\tau_{e,\kappa,s}$	Defined by equation (12)
Φ	$\Phi = \mathring{R} + \sum_i s_i \epsilon_i$
ω	Angular frequency of applied electric field
ω_p	Plasma frequency, $\omega_p = 2\pi f_p = 2\pi(9 n_e^{1/2})$
$\mathring{\Omega}$	Ohmic heating, equation (38)

Subscripts

$( )_e$	Quantities associated with electrons
$( )_{el}$	Values for elastic collisions
$( )_{inel}$	Values for inelastic collisions
$\langle \rangle$	Average over velocity distribution
$\langle \rangle_o$	Average for a Maxwellian distribution
$( )_s$	Quantities associated with the s class of energy states; s identifies translational, rotational or vibrational degrees of freedom
$( )_\kappa$	Quantities associated with species κ

NOVEL METHOD FOR DETERMINATION OF ENERGY-LOSS FACTORS FOR SLOW ELECTRONS IN HOT GASES

by S. T. Demetriades
STD Research Corporation, Pasadena, California 91106

SUMMARY

The energy-loss factor for slow electrons in hot gases is determined by a new method that employs a high-frequency (2.45 GHz) electric field to elevate the temperature of the electrons above the temperature of the gas and a Langmuir probe to determine the electron temperature. The electron energy-loss factor δ_κ in a given gas κ is then determined by measuring the rate of change of the electron temperature with the high-frequency power used to illuminate the plasma. The determination of δ_κ by this method does not require knowledge of the collision cross-sections for momentum transfer or of other transport coefficients or of the number densities of the electrons and neutral particles present. An arc heater was used to generate the hot gas. The energy state of the gas was determined spectroscopically.

The values of δ_κ obtained by this method are in agreement with theory for monatomic gases (e.g., argon). The values of the energy-loss factors δ_κ obtained for nitrogen and δ_{eff} obtained for N_2-O_2 mixtures (with oxygen concentrations up to 50%) are a reasonable extrapolation of the room temperature data available in the literature. It was found that δ_{N_2} ranges approximately from 3×10^{-4} at a gas temperature of 1700 °K to 7×10^{-4} at 5000 °K. The determination of electron energy-loss factors in mixtures is further complicated by the large number of variables; nevertheless for electrons in the temperature range between 2000 °K and 2500 °K in air at temperatures in the vicinity of 1700 °K it was found that $\delta_{air} \approx 3 \times 10^{-3}$.

It is concluded that this is a valid and accurate method for determining energy-loss factors since the experimentally obtained values are in essential agreement with theoretical predictions for various gases over a range of more than two orders of magnitude in the loss factor.

INTRODUCTION

Many non-linear phenomena in plasma dynamics and electromagnetism as well as the processes of excitation or de-excitation of atomic or molecular particles by electron impact are characterized, and to a large extent, controlled, by the electron energy-loss factor, a quantity that determines the rate of energy transfer from electrons to heavy particles and expresses the fraction of energy that an electron loses, on the average, per collision with the heavy particles.

Development of a simple, reliable and direct method for the determination of electron energy-loss factors in hot gases that permits presentation of the results in a concise and convenient form (e. g., as a function of electron and gas temperature) is the purpose of this investigation.

The energy-loss factor for slow electrons in hot gases is determined by a new method that employs a high-frequency electric field to elevate the temperature of the electrons above the temperature of the gas and a Langmuir probe to determine the electron temperature. The electron energy-loss factor δ_κ in a given gas κ is then determined by measuring the rate of change of the electron temperature with the high-frequency power used to illuminate the plasma (ref. 1).

The experimental results obtained so far offer evidence that this method is capable of meeting the objectives: it is demonstrated that the proposed method works and gives results that can withstand all reasonable checks for validity, that the energy state of the gas can be adequately established and that the results can be obtained and presented in a concise and convenient form.

In this method for determining the electron energy-loss factor in hot gases all important measurements are dc and the energy-loss factor is uncoupled from (a) the collision frequency for momentum transfer, or (b) the drift velocity, the mobility and the electron diffusion coefficient and hence can be determined independently of particle densities, collision cross-sections for momentum transfer, and other transport parameters.

Experimental data on the value of δ_K as a function of electron and gas temperature obtained by this technique are in a form consistent with the powerful new theoretical treatments of non-linear plasma dynamics now becoming available (e. g., such as the theoretical work of Argyropoulos et al., ref. 2) and are essential for obtaining accurate quantitative results from these theories.

For these reasons a recapitulation of some of the pertinent basic theoretical expressions of non-linear plasma dynamics is appropriate and useful.

ELECTRON ENERGY TRANSPORT AND THE ENERGY-LOSS FACTOR

Success in any scheme to describe quantitatively the electron-energy dependent non-linearities in a plasma rests on the degree of understanding that has been achieved concerning the mechanisms of electron energy transport in high-temperature gases.

A consistent scheme for obtaining a closed set of transport equations in a plasma was given by Demetriades and Argyropoulos (ref. 3). Using their notation, repeated here in the list of symbols, it can be shown (ref. 4) that the third moment of the Boltzmann equation for electrons (i.e., the equation obtained by multiplying the Boltzmann equation by $\frac{1}{2} m_e w_e^2$ and integrating over velocity space) results in the so-called "thermal energy balance" equation which is given by

$$\frac{\partial}{\partial t}\left(\frac{3}{2} p_e\right) + \nabla \cdot \left(\frac{3}{2} p_e \vec{U} + \vec{q}_e\right) + \overleftrightarrow{\pi}_e : \nabla \vec{U} =$$

$$= \rho_e \vec{W}_e \cdot \left[\frac{e_e}{m_e} \left(\vec{E} + \vec{U} \times \vec{B}\right) - \frac{d\vec{U}}{dt} \right] + R_e^{(2)} \qquad (1)$$

Equation (1) is also obtained by subtracting the dot product of the momentum equation for the electrons and the flow velocity $\vec{U}$ from the total energy equation for the electrons (whence the term "thermal energy

balance" equation). In equation (1) the subscript e refers to electrons and the collisional energy exchange integral $R_e^{(2)}$ is defined by the general expression*

$$R_e^{(2)} \equiv \int_{w_e} \frac{1}{2} m_e w_e^2 \left(\frac{\partial f_e}{\partial t}\right)_c d\vec{w}_e \qquad (2)$$

where f_e is the electron distribution function.

The elastic part of this integral (i.e., the translational energy exchange) can be readily obtained by the methods of reference 3 or references 4, 5 and 6 and reduces exactly to the form

$$\left[R_e^{(2)}\right]_{el} = -\frac{3}{2} k n_e \sum_{\kappa} (2m_e/m_\kappa)(T_e - T_\kappa) \tau_{e,\kappa}^{-1} \qquad (3)$$

under the assumption that the isotropic part of the distribution functions both for the electrons and for all heavy components κ is Maxwellian. Thus equation (3) as written above is also a result of the general elastic collision integral expression for $R_a^{(n)}$ given by equation (3) of reference 3.

In addition to the elastic part given by equation (3), one generally considers the following inelastic collisional processes of energy exchange between free electrons and heavy particles:

(1) Excitation of rotational and vibrational levels in molecular species
(2) Excitation of electronic states of the heavy particles
(3) Collisions leading to dissociation, ionization or recombination or the creation of metastable species with lifetimes much longer than the lifetimes of the excited particles of item (2)

* The identity of this definition and that appearing as equation (3) of reference 3 may be established by use of known properties of molecular collisions. See, for example, Hirschfelder, J. O.; Curtiss, C. F.; and Bird, R. B.: Molecular Theory of Gases and Liquids, J. Wiley & Sons, New York, (1954) p. 460.

(4) "Second order" impacts that result in the transfer of the energy of the excited or metastable particle to the incoming electron

As shown by the authors of reference 7, the inelastic energy losses to rotational and vibrational levels can be adequately taken into account by substituting δ_κ for $2m_e/m_\kappa$ in equation (3) and using a measured value of δ_κ (such measurements are described in reference 1).

Concerning the excitation of electronic states, use can be made of the fact that in most plasmas of interest to this investigation the excited levels of atoms or molecules are generally in instantaneous equilibrium with the free electrons. [In these plasmas, while the electrons, atoms and molecules experience energy exchange among one another, the ultimate loss of energy from the system is due to radiation.] Therefore, the appropriate portion of the collisional energy losses of free electrons (i.e., that portion of the energy lost by an electron upon impact with an atom or molecule that goes into exciting electronic levels of the heavy particle) can be equated to the radiative losses $\dot{R}$ from excited states of the heavy particles at the electron temperature (see for example reference 8).

Finally, collisional energy losses due to ionizing or dissociating collisions or collisions leading to the creation of metastable states (free radicals, etc.) or energy gains due to the reverse reaction mechanisms, are expressed in terms of the rate s_i of each reaction (in units of number of reactions per unit volume per unit time) and each characteristic energy or potential ϵ_i (in units of energy per reaction). The sign of ϵ_i depends of course on whether the electron loses or gains energy by that particular mechanism.

Thus the total (elastic + inelastic) collisional exchange of energy between electrons and heavy particles can be written as the sum of equation (3) and the inelastic contributions just enumerated, in the form

$$R_e^{(2)} = \left[R_e^{(2)}\right]_{el} + \left[R_e^{(2)}\right]_{inel} \equiv \int_{w_e} \frac{1}{2} m_e w_e^2 \left(\frac{\partial f_e}{\partial t}\right)_c d\vec{w}_e$$

$$= -\frac{3}{2} k n_e \sum_{\kappa} \delta_{\kappa} (T_e - T_{\kappa}) \tau_{e,\kappa}^{-1} - \dot{R} - \sum_i s_i \epsilon_i \qquad (4)$$

The quantity δ_{κ} accounts for the energy lost by the electron in elastic collisions (i.e., involving translational degrees of freedom only) as well as in some inelastic collisions (i.e., involving rotational and vibrational degrees of freedom of the heavy particles). The quantity δ_{κ} is thus a characteristic energy-loss parameter that has the meaning of an average fraction of the energy difference $\frac{3}{2} k (T_e - T_{\kappa})$ transferred in collisions between the electron and the heavy particles κ within a time $\tau_{e,\kappa}$. For example, when the heavy particles are at equilibrium and have only one, well-defined temperature $T_{\kappa} = T_g$, the difference between the average internal energy of the electrons and the average internal energy of the heavy component κ is $\frac{3}{2} k (T_e - T_g)$. Then if the heavy particles are, for example, monatomic, optically unexcited and unexcitable, chemically stable and inert (i.e., if they behave like hard inert spheres) the electron impact is perfectly elastic and the elastic energy loss factor $\delta_{\kappa,el}$ is the fraction of this energy difference that is lost on the average by an electron in each elastic collision with component κ. Thus $\delta_{\kappa,el} = 2m_e/m_{\kappa}$.

In a single-component gas or plasma at equilibrium where again T_{κ} and T_g are equal, and $\dot{R}$ as well as $\sum_i s_i \epsilon_i$ are known, the appropriate inelastic energy-loss factor δ_{κ} can be determined experimentally, for example, by obtaining all other quantities and using equations (1) and (4).

In a multicomponent gas or plasma where all the heavy components are at equilibrium at the same temperature $T_{\kappa} = T_g$, we can write equation (4) in the form

$$R_e^{(2)} = -\frac{3}{2} k n_e \nu_t \delta_{eff} (T_e - T_g) - \dot{R} - \sum_i s_i \epsilon_i \qquad (5)$$

where ν_t is defined in reference 3 as

$$\nu_t \equiv \sum_{\kappa \neq e} \tau_{e,\kappa}^{-1} = \frac{4}{3} \sum_{\kappa \neq e} \nu_{e,\kappa} \qquad (6)$$

and δ_{eff} is defined in reference 1 as

$$\delta_{eff} \equiv (1/\nu_t) \sum_{\kappa} \delta_{\kappa} \tau_{e,\kappa}^{-1} \tag{7}$$

Again δ_{eff} can be obtained experimentally [either directly from equations (1) and (5) by obtaining all other quantities or from the δ_{κ}'s for each component and the mixture rule given by equation (7)].

Finally, in a multicomponent gas or plasma where the heavy components are at different translational, rotational and vibrational temperatures $T_{\kappa,tr}$, $T_{\kappa,rot}$ and $T_{\kappa,vib}$ respectively, we can write

$$R_e^{(2)} = -\frac{3}{2} k n_e \sum_{\kappa} \sum_{s} \delta_{\kappa,s} (T_e - T_{\kappa,s}) \tau_{e,\kappa}^{-1} - \dot{R} - \sum_{i} s_i \epsilon_i \tag{8}$$

where the subscript s identifies translational (tr), rotational (rot) or vibrational (vib) temperatures or corresponding contributions to δ_{κ}.

Once more the values of the coefficients $\delta_{\kappa,s}$ can be obtained experimentally provided $\dot{R}$ and $\sum_i s_i \epsilon_i$ are known or measurable. An effective energy-loss factor δ_{eff} can now be defined as

$$\delta_{eff} \equiv \sum_{\kappa} \sum_{s} \delta_{\kappa,s} \cdot \frac{\tau_{e,\kappa}^{-1}}{\nu_t} \cdot \frac{T_e - T_{\kappa,s}}{T_e - T_n} \tag{9}$$

where the double summation requires two normalization factors (i.e., ν_t and $T_e - T_n$) and T_n is <u>any</u> convenient reference temperature. Then we obtain

$$R_e^{(2)} = -\frac{3}{2} k n_e \nu_t \delta_{eff} (T_e - T_n) - \dot{R} - \sum_{i} s_i \epsilon_i \tag{10}$$

It should be remembered that the first term on the right-hand side of equation (10) represents the energy exchange between electrons and heavy particles in collisions that excite translational, vibrational and rotational

energy states. Hence this term involves all of the elastic and part of the inelastic energy exchange.

Note that the summation over the classes s of energy states where s = tr, rot, vib is equivalent to treating each class s of energy states of each species as a distinct and separate component.* When this is done, the first term on the right-hand side of equation (8) is analogous to and a direct extension of the simple expression for the translational energy transport, equation (3) above, derived from the theory presented by Demetriades and Argyropoulos, reference 3. The assignment of a temperature $T_{\kappa, s}$ to each state of each plasma component and the treatment of each state of each component as a different species is permitted on the basis of energy considerations. On the other hand, the collision frequency $\tau_{e,\kappa}^{-1}$ is excluded from summation over energy states since it characterizes momentum transfer only.

As an example, let us consider a mixture of nitrogen and oxygen where $T_{N_2, tr} = T_{N_2, rot} = T_{O_2, tr} = T_{O_2, rot}$ while $T_{N_2, vib} = T_{O_2, vib} = T_{vib}$ and $\delta_{N_2, tr} \approx \delta_{O_2, tr} < \delta_{N_2, rot} < \delta_{O_2, rot} \ll \delta_{N_2, vib} < \delta_{O_2, vib}$. Then by equation (9) the energy-loss factor for the mixture becomes

$$\delta_{eff} \approx \frac{T_e - T_{vib}}{T_e - T_n} \cdot \frac{1}{\nu_t} \cdot \sum_{\kappa} \delta_{\kappa, vib} \cdot \tau_{e,\kappa}^{-1} \qquad (11)$$

where $\kappa = N_2, O_2$. Then if we choose $T_n = T_{vib}$ for normalization purposes, we obtain expressions identical to equations (5) and (7) where, in this case, the appropriate heavy particle temperature, T_g, is the vibrational temperature.

It is important to note at this point that δ_{eff} (and δ_{κ} for all known species) is much smaller than unity.

---

* By class of energy states we mean the energy states that are associated with a particular degree of freedom. For example the vibrational energy class contains all the energy states that are associated with the vibrational degrees of freedom.

We can now proceed to make some statements illustrating and clarifying the use of equations (1) and (5), (8) or (10).

Use of the term $\dot{R}$ in equations (5), (8) or (10) implies that the quantity δ_κ, or more generally $\delta_{\kappa,s}$ excludes collisional excitation of bound electrons by free electrons. Use of the term $\dot{R}$ is based on the assumption that the population of the bound electronic levels is at equilibrium at the temperature of the free electrons T_e or, in other words, that the energy lost by the free electrons in the process of excitation of optical levels of heavy particles is equal to the energy lost by these heavy particles through radiation. Clearly, the quantity $\dot{R}$ is a complicated function of the geometry of the plasma (refs. 9 and 10) and the relative importance of the term $\dot{R}$ compared to the term containing the energy loss factor is greater in monatomic gases (where δ_κ is close to the elastic value $2m_e/m_\kappa$ and therefore quite small) than in diatomic gases (where δ_κ is usually many times greater than $\delta_{\kappa,el}$). Usually, however, even for monatomic gases there are ranges of T_e and T_g where the term containing δ_κ in equations (5), (8) or (10) is dominant and $\dot{R}$ can be safely neglected (e.g., see reference 11).

The other important term, $\sum_i s_i \epsilon_i$, appearing in equations (5), (8) or (10) may be the source of considerable confusion if it is not properly taken into account. For example it is easily seen that it can be both a source and a sink of electron energy (as would be the case for example when free electrons are picking up energy by becoming collision partners with metastables or third bodies in recombination reactions while at the same time they become collision partners in dissociative reactions). A reasonable estimate of the relative magnitude of this term within the control volume of the experiment will always be necessary when use is made of these equations.

A final point that must be clarified in this section is the relationship between collision cross-sections for momentum transfer and collision cross-sections for energy transfer. We define an "effective collision frequency for energy transfer" between electrons and the s-class of energy states of heavy particles of species κ in a manner completely analogous

to the definition in reference 3 of an "effective collision frequency for momentum transfer" $\tau_{a,\beta}^{-1}$, by the expression

$$\tau_{e,\kappa,s}^{-1} \equiv \frac{4}{3} n_\kappa \langle g_{e\kappa} \rangle_o Q_{e,\kappa,s} \equiv \frac{4}{3} \nu_{e,\kappa,s} \tag{12}$$

where $\langle g_{e\kappa} \rangle_o$ is the mean approach or relative speed between the electron and component κ (for Maxwellian velocity distribution of the two components at their respective kinetic or translational temperatures) and $Q_{e,\kappa,s}$ is the "effective collision cross-section for energy transfer" between electrons and the s-class of energy states of species κ. This definition is entirely consistent with the transport theory formulation and methodology of reference 3.

Now we consider the meaning of the term $R_e^{(2)}$. It can be thought of as a collisional energy source or sink for the electrons (in the same manner for example, that $R_e^{(1)}$ which is treated in reference 3, can be thought of as a collisional force*) and represents a power density. Therefore, in a manner analogous to the make-up of $R_e^{(1)}$, the first term on the right-hand side of equation (10) must be made up of an energy difference term, a number density term, and a collision frequency. A look at the elastic expression for $R_e^{(2)}$, equation (3), should suffice to convince us that the energy difference term is $\frac{3}{2} k(T_e - T_\kappa)$, the number density term is n_e and therefore the effective collision frequency for energy transfer can also be defined by

$$\tau_{e,\kappa,s}^{-1} \equiv \delta_{\kappa,s} \tau_{e,\kappa}^{-1} \equiv \frac{4}{3} \delta_{\kappa,s} \nu_{e,\kappa} \tag{13}$$

Therefore, using the result of reference 3 for the effective collision frequency for momentum transfer given by $\tau_{e,\kappa}^{-1} = \frac{4}{3} n_\kappa \langle g_{e\kappa} \rangle_o Q_{e\kappa}$ we obtain

* $R_e^{(1)}$ is defined by an integral similar to that for $R_e^{(2)}$, equation (2), except that $m_e \vec{w}_e$ replaces $\frac{1}{2} m_e w_e^2$. See equation (3) of reference 3.

$$Q_{e,\kappa,s} = \delta_{\kappa,s} Q_{e\kappa} \tag{14}$$

From equations (10) and (13) we see that the total effective collision frequency for energy transfer ν_{te} is equal to $\nu_t \delta_{eff}$ and not to the simple sum $\sum_{\kappa} \sum_{s} \tau_{e,\kappa,s}^{-1}$ unless all $T_{\kappa,s} = T_n$. Since electron collisions with each component κ in the energy class s contribute a fraction of the total energy exchange that must be weighted by the temperature ratio $(T_e - T_{\kappa,s})/(T_e - T_n)$, it follows that the total effective collision frequency for energy transfer ν_{te} is given by the expression

$$\nu_{te} = \sum_{\kappa} \sum_{s} \tau_{e,\kappa,s}^{-1} \left(\frac{T_e - T_{\kappa,s}}{T_e - T_n} \right) = \nu_t \delta_{eff} \tag{15}$$

It must be emphasized that equations (14) and (15) are really consequences of the definitions given by equations (12) and (13) and although they add nothing new to our knowledge they help maintain the consistency of our results and underscore the points of similarity and/or difference with other theories or investigations.

DESIGN OF THE EXPERIMENT

Under steady-state conditions ($\partial p_e/\partial t = 0$, $\partial \vec{U}/\partial t = 0$) in a flow field with negligible gradients of axial velocity, electron concentration and temperature (i.e., $\nabla \cdot [3 p_e \vec{U}/2 + \vec{q}_e] + \overleftrightarrow{\pi} : \nabla \vec{U} = 3 \vec{U} \cdot \nabla k n_e T_e/2 + 3 p_e \nabla \cdot \vec{U}/2 + \nabla \cdot \vec{q}_e + p_e \nabla \cdot \vec{U} - \overleftrightarrow{\tau}_e : \nabla \vec{U} \approx 0$ since $\partial n_e/\partial x = \partial T_e/\partial x = \partial U_x/\partial x \approx 0$) the electron thermal energy balance, equation (1), becomes

$$\vec{J}_e \cdot (\vec{E} + \vec{U} \times \vec{B}) = \frac{3}{2} \kappa n_e \nu_t \delta_{eff} (T_e - T_n) + \dot{R} + \sum_i s_i \epsilon_i \tag{16}$$

where δ_{eff} is defined by equation (9). When $\vec{U} \times \vec{B}$ is negligible and the electric field is constant with time we obtain, in the first approximation (ref. 3)

$$\vec{J}_e \cdot \vec{E} = \frac{e^2 n_e E_o^2}{2 m_e \nu_t} = \frac{3}{2} k n_e \nu_t \delta_{eff} (T_e - T_n) + \dot{R} + \sum_i s_i \epsilon_i \qquad (16a)$$

The use of this expression to determine δ_{eff} has two major disadvantages: (1) the dc electric field cannot penetrate the plasma without a significant associated current, which results in local heating or breaking-down of the gas and changes the homogeneity of its properties and (2) the energy-loss factor is coupled with the square of the total collision frequency and it becomes difficult to separate these two transport parameters and prevent uncertainties in ν_t from affecting the determination of δ_{eff}. Both of these difficulties can be avoided by using an rf electric field.

By using equation (16) and the methods of Ginzburg and Gurevich (ref. 7, pp. 119 ff.) it is now possible to show that when $\vec{B} = 0$ in a high-frequency electric field ($E = E_o \cos \omega t$, $\omega \equiv 2 \pi f$) the electron energy balance reduces to

$$\vec{J}_e \cdot \vec{E} = \frac{e^2 n_e \nu_t E_o^2 (1 + \epsilon) \Pi}{2 m_e (\omega^2 + \nu_t^2)} = \frac{3}{2} k n_e \nu_t \delta_{eff} (T_e - T_n) + \dot{R} + \sum_i s_i \epsilon_i \qquad (16b)$$

Therefore the difference between the electron temperature T_e and the reference gas temperature T_n in the absence of radiation ($\dot{R} = 0$) and secondary energy exchange processes ($\sum_i s_i \epsilon_i = 0$) is given by

$$T_e - T_n = \frac{e^2 E_o^2 (1 + \epsilon) \Pi}{3 k \delta_{eff} m_e (\omega^2 + \nu_t^2)} \qquad (17)$$

When $\dot{R}$ and $\sum_i s_i \epsilon_i$ are not negligible we obtain

$$T_e - T_n = \frac{e^2 E_o^2 (1 + \epsilon) \Pi}{3 k \delta_{eff} m_e (\omega^2 + \nu_t^2)} - \frac{2}{3 k n_e \nu_t \delta_{eff}} \left[\dot{R} + \sum_i s_i \epsilon_i \right] \qquad (17a)$$

Generally, when $T_e - T_n \neq 0$ in the absence of an electric field, a

steady-state temperature difference is sustained by radiative energy losses or secondary energy exchange processes. Equation (17) is valid only if the effects of the electric field dominate.

The quantity ϵ (which arises from the time-dependence of the electric field and is given explicitly in reference 7) is usually much less than unity when $\omega >> \nu_t$. The quantity Π arises from considering the frequency and electron-temperature dependent higher order approximations to the kinetic coefficients and is also given explicitly in reference 7. It is always very close to unity when (a) the predominant collisions are electron-neutral particle collisions or (b) the predominant collisions are electron-ion collisions but at the same time $\omega^2 >> \nu_t^2$. The factor Π differs significantly from unity (and therefore influences substantially the electron temperature) only in the case of collisions with ions at low frequencies of the applied electric field ($\omega \lesssim \nu_t$) and also in the region of gyro resonance if, contrary to the situation treated here, the magnetic field is non-zero.

Equation (17) immediately suggests a method for the determination of δ_κ or δ_{eff}: If a gas or plasma in which $\dot{R} = \sum_i s_i \epsilon_i = 0$ is illuminated by a high-frequency electric field such that $\omega^2 >> \nu_t^2$ its energy-loss factor can be obtained independently of the electron collision frequency and all other transport coefficients, by measuring the rate of change of electron temperature with the amplitude of the illuminating electric field while the gas temperature $T_{\kappa, s}$ and also of course the reference or normalization temperature T_n, remain constant. (The condition of constant $T_{\kappa, s}$ implies that the illuminating electric field must heat the electrons but not the gas. This is virtually assured if the degree of ionization is small, especially in a flow system.) Assuming $\omega^2 >> \nu_t^2$ and differentiating equation (17) with respect to the electron temperature we obtain

$$\delta_{eff} = \frac{2e^2 E_o}{3 k m_e \omega^2} \left[\frac{\partial E_o}{\partial T_e} - \frac{E_o}{2} \cdot \frac{\partial (\ell n \, \delta_{eff})}{\partial T_e} \right] \qquad (18)$$

If P is the power fed into the appropriately constructed and terminated illumination cavity (propagating primarily the TE_{10} mode as described in Appendix A), Z is the impedance of the gap (377 Ω for vacuum, but see Appendix A for values applicable in our case), and A_r is the appropriate cross-sectional area of the beam or gap (in our case the area perpendicular to the wave propagation axis as described in Appendix A), equation (18) can be transformed to

$$\delta_{eff} = \frac{e^2}{3km_e\omega^2}\left(\frac{4Z}{A_r}\right)\left(\frac{\partial P}{\partial T_e}\right)\cdot\left[1 - \frac{\partial T_e}{\partial \ell nP}\cdot\frac{\partial(\ell n\delta_{eff})}{\partial T_e}\right] \qquad (19)$$

When the electron energy-loss factor remains constant or very nearly constant with T_e (as it does, for example, in diatomic gases over narrow ranges of T_e where the electron energy remains below the threshold for exciting the next higher energy-absorption mechanism in the heavy particle) we can write

$$\delta_{eff} = \frac{2e^2\nu_c}{3km_e\omega^2}\left(\frac{dE_o}{dT_e}\right) = \frac{e^2}{3km_e\omega^2}\left(\frac{4Z}{A_r}\right)\left(\frac{dP}{dT_e}\right) \qquad (20)$$

A convenient determination of the electron energy-loss factor by means of equations (18), (19) or (20) can be carried out by measuring the electron temperature T_e in the cavity as a function of the incident power of illumination P and obtaining $dT_e/dE_o = (dE_o/dT_e)^{-1}$ or $dT_e/dP = (dP/dT_e)^{-1}$. The measurement of P is trivial; the measurement of T_e is not.

The alternative method of determining δ_{eff} from equation (17) by measuring the rate of change of electron temperature with the frequency ω at $\omega^2 >> \nu_t^2$ was also considered. Since, however, it is far more convenient to change P by one or more orders of magnitude (to correspond to desirable conditions for different gases with δ_{eff}'s varying by as much as three orders of magnitude) than ω, this alternative approach was for the time being abandoned.

In both methods, however, the energy-loss factor is inferred directly from measurements of macroscopic quantities. Independent determination of such parameters as cross-sections, electron mobility and particle densities are not required.

Physical Constraints Placed on the Experiment

Choice of a method for measuring T_e must be governed by several criteria: it must be compatible with the assumptions made in deriving equations (18), (19) or (20) and with the environment, geometry, other constraints of the experiment; it must introduce the minimum number of additional conditions; it must be simple, reliable and economical; it must not interfere with the other measurements nor should the other measurements interfere with it; and it must yield the maximum possible useful information. However, whatever the criteria for choosing a method for measuring T_e, they are overshadowed by the necessity to establish first the existence of an electron temperature, i.e., to ensure a Maxwellian thermal energy distribution for the electrons in the gas under consideration.

We discern therefore a certain hierarchy of conditions and constraints that are essential to the success of the experiment. They arise from the basic requirement for the existence of electrons with a well-defined temperature in a hot gas and the operational requirements of heating these electrons with an rf electric field and measuring their temperature.

The first of these constraints that have to be met is the one that assures a Maxwellian electron energy distribution. The criterion for Maxwellian electrons is that the collision frequency for energy transfer between electrons, should be larger than the total collision frequency for energy transfer between electrons and neutrals (ref. 7). The energy-loss factor for electron-electron collisions is $\delta_e = \frac{1}{2}$. (This value for the energy-loss factor is obtained from classical collision theory for two particles of equal mass. The general formula is $\delta_\kappa = 2m_e m_\kappa/(m_e + m_\kappa)^2$ which reduces to $2m_e/m_\kappa$ for $m_\kappa >> m_e$ and to $(1/2)$ for $m_e = m_\kappa$.)

Therefore, the effective collision frequency for energy transfer among electrons is $\tau_{e,e,e}^{-1} = \frac{1}{2}\tau_{e,e}^{-1}$ where $\tau_{e,e}^{-1}$ is the effective collision frequency for momentum transfer among electrons. From equation (10) the total effective collision frequency for energy transfer between electrons and all heavy particles is $\nu_t\delta_{eff}$. Therefore, the ratio R_M of these two quantities is given by

$$R_M = \frac{\frac{1}{2}\tau_{e,e}^{-1}}{\nu_t\delta_{eff}} = \frac{1}{2}\tau_{e,e}^{-1}\left[\sum_{\kappa}\delta_\kappa\tau_{e,\kappa}^{-1}\right]^{-1} \tag{21}$$

where equation (7) is used for $\nu_t\delta_\kappa$.

If we use the collision cross-section for momentum transfer between charged species given as equation (24) in reference 3, we obtain ($\kappa \neq e$)

$$R_M \approx 6\times 10^7\left(\frac{11620}{T_e}\right)^2\left\{\sum_{\kappa}\frac{n_\kappa}{n_e}\left(\frac{Q_{e,\kappa}}{10^{-20}}\right)\left(\frac{\delta_\kappa}{10^{-4}}\right)\right\}^{-1} \tag{22}$$

in mks units. The electron energy distribution is Maxwellian when the magnitude of the parameter R_M satisfies the inequality $R_M >> 5$ (ref. 7). It must be noted that at high electron velocities, i.e., at the tail of the distribution function, deviations from Maxwellian are significant even at $R_M \approx 50$. On the other hand, at low electron velocities (i.e., at low electric fields) the constraint $R_M >> 5$ can be relaxed considerably and in our case we can expect a sensibly Maxwellian distribution even at $R_M \approx 1$.

Clearly, the most important result of the constraint imposed by $R_M >> 5$ is that the experiment must be operated in an environment where n_e/n_κ is not less than approximately 10^{-7} for monatomic gases and 10^{-6} or higher for polyatomic gases. It is worth noting that any enhancement of the degree of ionization that occurs because of the elevation of T_e makes it easier to meet this constraint.

When n_e is specified by some other constraint or design consideration, this constraint serves to specify the maximum permissible neutral particle density n_a.

The second of these constraints involves the limitation on the

electron number density imposed by the requirement that the illuminating high-frequency electric field must penetrate the plasma. The condition $\omega > \omega_p \equiv 2\pi f_p$, where ω_p is the critical plasma frequency in radians/sec given by $f_p = 9(n_e)^{1/2}$ in Hz, when n_e is in electrons/m^3, ensures that the high-frequency electric field will penetrate the plasma and imposes an upper limit on the electron concentration given by

$$n_e \leq f^2/81 = \omega^2/324\pi^2 \tag{23}$$

where the frequency of the applied electric field is f in Hz or ω in rad/sec. Any enhancement of the electron number density that occurs because of the elevation of the electron temperature makes it tougher to meet this constraint and great care should be taken to make sure it is observed. (See also the discussion of the eighth constraint.)

The third of these constraints arises from the requirement that $\omega^2 >> \nu_t^2$ and imposes an upper limit on the neutral particle density n_a. If we consider the case where only one neutral species is present and only electron-neutral collisions for momentum transfer are important, the neutral particle density must satisfy the inequality

$$n_a^2 << \frac{9}{16}\left(\frac{\pi m_e}{8kT_e}\right)\frac{\omega^2}{Q_{ea}^2} = 1.46 \times 10^{-8}\,\frac{\omega^2}{Q_{ea}^2 T_e} \tag{24}$$

obtained by combining special forms of equations (6) and (12). In equation (24) the quantity Q_{ea} is the collision cross-section for momentum transfer between electrons and neutral particles of species a, m_e is the mass of the electron and the mean approach speed between electrons and neutral particles $\langle g_{ea} \rangle_o$ in equation (12) has been taken to be $\langle g_{ea} \rangle_o = (8kT_e/\pi m_e)^{1/2}$.

Note that although the first constraint can be interpreted to specify the minimum permissible degree of ionization, the second and third constraints cannot be combined and interpreted to specify the maximum permissible degree of ionization. In fact, the second and third constraints must be considered independently and to ensure that they as

well as the first constraint are met, the number densities of electrons and neutrals must be controlled, as far as possible, independently of each other.

From this point, in order to make further progress in the design of the experiment we must specify the method for the production of the hot gas or plasma with independently controlled electron and neutral number densities and we must specify the method of measurement of the electron temperature.

Since a convenient source of hot gas or plasma of independently controlled enthalpy, electron number density and neutral number density is an arcjet expanding into a vacuum chamber, it was decided to combine such a method of production of electrons and hot gas with the most convenient and widely-used method of obtaining a spatially-resolved electron temperature in plasmas of this type — the Langmuir probe. A considerable body of experience has accumulated over the years in the use of Langmuir probes to measure electron temperatures in plasma flows produced by arcjets (e.g., refs. 12, 13 and 14). A cylindrical probe appears especially suitable to the conditions expected in this experiment (ref. 12). The use of Langmuir probes for accurate determination of electron temperatures is not plagued with the difficulties associated with the use of these probes for precise measurement of the electron number densities. Nevertheless, use of the data obtained by these probes to establish order-of-magnitude values of the electron number densities is a welcome addition to the diagnostic information required to establish confidence in these experiments. Finally, the data obtained in each determination of T_e by these probes can establish at a glance the existence or non-existence of a Maxwellian electron energy distribution and thereby provide a check on the validity of the measurements and tangible proof that the first constraint is adequately met.

Use of this particular method for obtaining T_e introduces additional constraints. Observance of these constraints ensures that the data obtained by the probe can be interpreted unambiguously to yield the electron temperature.

Thus the fourth constraint requires that the Langmuir probe diameter D_p must not be larger than the mean free path λ_e of the electrons. This condition implies that the neutral particle density must satisfy the inequality

$$n_a \leq 1/(D_p Q_{ea}) \tag{25}$$

and for $D_p = 0.001$ m we must ensure

$$n_a \leq 10^3 Q_{ea}^{-1}$$

The fifth constraint requires that the diameter of the probe should be much larger than the electron Debye length λ_D. This condition implies

$$D_p >> \lambda_D = \left(\frac{\epsilon_o k T_e}{n_e e^2}\right)^{1/2} = 69.01 \left(\frac{T_e}{n_e}\right)^{1/2} \tag{26}$$

in mks units and for $D_p = 0.001$ m we must ensure that

$$n_e >> 4.77 \times 10^9 T_e$$

The constraints prescribed by these two inequalities are not particularly hard to satisfy and conclude the demands made on the experimental environment by the cylindrical Langmuir probe when used to determine T_e.

All other operational constraints are imposed by the technique we have chosen for heating the electrons.

Thus the sixth constraint requires that the characteristic flow time of the plasma across the waveguide must be much larger than the excitation or relaxation time for the electron temperature (or, in other words, that the time-of-flight of the electrons must be large compared to the electron temperature rise time). Observance of this constraint ensures that the electrons will indeed be heated in the waveguide since

their time-of-residence in it will be much longer than the time required to heat them. Since the electron energy excitation time is at least as fast as the relaxation time $1/\nu_t\delta_{eff}$ (ref. 7), if the flow velocity of the plasmajet is U and the length of the waveguide in the flow direction is a, this condition is satisfied when

$$\frac{a}{U} > \frac{1}{\nu_t \delta_{eff}} \tag{27}$$

This constraint imposes either a lower limit on n_a (or a minimum permissible length, a, or a maximum permissible flow velocity U) given by

$$n_a > \frac{U}{a\,\delta_{eff} Q_{ea} \langle g_{ea} \rangle_o} \tag{28}$$

where $\langle g_{ea} \rangle_o = (8kT_e/\pi m_e)^{1/2} = 6.213 \times 10^3\, T_e^{1/2}$. When this constraint is satisfied, we can be certain that at the probe the electron temperature corresponds to the electric field E_o and equations (18) or (19) apply. Since the dimension a and the flow velocity U are specified by waveguide and arcjet design considerations, this inequality also sets a lower limit on n_a, which is usually compatible with the requirements placed on n_a by the first and third constraints.

The seventh constraint arises from the need to obtain an elevation $\Delta T_e = T_e - T_{e1}$ of the electron temperature above some inital electron temperature T_{e1} that is equal to or larger than a certain minimum $(\Delta T_e)_{min}$. This value of $(\Delta T_e)_{min}$ is usually imposed by considerations that have to do with the precision of the measurement of T_e. Clearly, for example, we must obtain a ΔT_e that is larger than the minimum detectable electron temperature elevation with the Langmuir probe apparatus used in the experiment. Moreover, this ΔT_e must be higher than the probable error in the measurement of the electron temperature to ensure accurate results (see Appendix B). This constraint on a minimum allowable ΔT_e imposes a lower limit E_{min} on the amplitude E_o of the electric field. If we neglect the dependence of δ_{eff} on T_e, we

obtain from equation (17) for $\omega^{\omega} >> \nu_t$ an expression for E_{min} in terms of $(\Delta T_e)_{min}$ given by

$$E_{min} = \left(\frac{3 k m_e \omega^2 \delta_{eff}}{e^2}\right)^{1/2} \left[T_{e1} + (\Delta T_e)_{min} - T_n \right]^{1/2}$$

$$= 3.83 \times 10^{-8} \delta_{eff}^{1/2} \omega \left[T_{e1} + (\Delta T_e)_{min} - T_n \right]^{1/2} \qquad (29)$$

The equivalent power increment $(\Delta P)_{min}$ required to produce $(\Delta T_e)_{min}$ is given by equation (19) as

$$(\Delta P)_{min} = 1.47 \times 10^{-15} \omega^2 \delta_{eff} \left(\frac{A_r}{4Z}\right) (\Delta T_e)_{min}$$

For example, when $\delta = 10^{-4}$, $\omega = 1.54 \times 10^{10}$ rad/sec = 2.45 GHz and $(\Delta T_e)_{min} = 100\ ^{o}K$ we obtain $E_{min} = 58.9$ V/m. Observance of the seventh constraint is ensured when

$$E_o = 3.83 \times 10^{-8} \delta_{eff}^{1/2} \omega (T_{e1} + \Delta T_e - T_n)^{1/2} \geq E_{min} \qquad (30)$$

We repeat here that the precise value of the required $(\Delta T_e)_{min}$ and therefore also of E_{min} depends on the accuracy in measuring T_e obtainable with the apparatus and on the precision required in the determination of δ_{eff} (see Appendix B).

The eighth constraint requires that the effect of the high frequency electric field on the plasma should be kept sufficiently small so that equation (17) remains valid and/or the influence of the electric field on the experiment (including the measurement of T_e) remains easily calculable (refs. 1 and 7). For example, if the rates of ionization are such that, while the gas is in the test section, the production of ion pairs is negligible, neither the validity of equation (17) nor the second constraint are violated for almost any practical value of E_o at $f \geq 2.45$ GHz. However, suppose E_o increases above the value of the characteristic plasma field E_p given in the first approximation by

$$E_p = \left[3kT_e \frac{m_e}{e^2} \delta_{eff} (\omega^2 + \nu_t^2)\right]^{1/2}$$

$$= 3.83 \times 10^{-8} \left[\delta_{eff} T_e (\omega^2 + \nu_t^2)\right]^{1/2} \quad (31)$$

Then it is possible, depending on how well the conditions of the first constraint are satisfied, that the electron velocity distribution function deviates from Maxwellian, especially at the high-energy tail (ref. 7). To avoid any such possible complications it is sometimes advisable to operate the experiment so that the amplitude of the applied electric field satisfies the condition

$$E_o \leq E_p \quad (32)$$

This constraint is not rigid for all conditions and should be used only when there is danger of violating the first constraint. For example, when $\delta_{eff} = 10^{-4}$ and $\omega = 1.54 \times 10^{10}$ rad/sec, we obtain $E_p = 5.9\, T_e^{1/2}$ V/m and $\omega^2 > \nu_t^2$. Therefore, an electric field amplitude equal to or less than a few hundred volts per meter is indicated in cases where there is any difficulty in establishing and/or maintaining a Maxwellian electron velocity distribution.

A combination of equations (30), (31) and (32) gives for $\omega^2 > \nu_t^2$

$$\left[T_{e1} + (\Delta T_e)_{min} - T_n\right]^{1/2} \leq \frac{E_o}{3.83 \times 10^{-8} \omega \delta_{eff}^{1/2}} \leq (T_{e1} + \Delta T_e)^{1/2} \quad (33)$$

and it is clear that although the seventh and eighth constraints can always be made compatible by proper choice of $(\Delta T_e)_{min}$ and E_o, an attempt must be made to carry out the experiment with as small an E_o or a $\Delta T_e / T_{e, E=0}$ (or, at least, as small a ΔT_e) as possible. The additional advantage of this condition, i.e. of operation as close as possible to $(\Delta T_e)_{min}$, is that it allows us to observe the variation of δ_{eff} with T_e in fine detail.

When the experiment is operated under conditions that satisfy the eighth constraint (i. e., with electric fields less than a few hundred V/m) one would expect that the additional constraints of operation at an electric field that is smaller than the breakdown potential of the gases involved (ninth constraint) and smaller than the critical electric field above which binary theory is questionable (tenth constraint), are also satisfied (refs. 1, 7 and 15).

The eleventh constraint arises from the requirement that the elevation of the electron temperature by the applied electric field should not be so small that any energy losses or gains experienced by the electron due to the existence of small but finite terms of the form $\partial \dot{R}/\partial T_e$ and $\partial \Sigma s_i \epsilon_i / \partial T_e$ are significant compared to the term $(3/2) k n_e \nu_t \delta_{eff}$, while, at the same time, ΔT_e should not be so high that the variation of δ_{eff} with T_e is masked. If we define $\partial \Phi / \partial T_e \equiv \partial \dot{R}/\partial T_e + \partial \sum_i s_i \epsilon_i / \partial T_e$ we observe from equation (16b) that, for $\omega^2 >> \nu_t^2$,

$$\left(\frac{e^2 n_e \nu_t E_o}{m_e \omega^2}\right) \frac{\partial E_o}{\partial T_e} = \frac{3}{2} k n_e \nu_t \delta_{eff} + \frac{\partial \Phi}{\partial T_e} \tag{34}$$

and therefore the first part of this constraint yields

$$\Delta T_e >> \frac{2 \Delta \Phi}{3 k n_e \nu_t \delta_{eff}} \tag{35}$$

This inequality implies that the major part of the ohmic heating goes into maintaining the electron temperature elevation ΔT_e.

The second part of this constraint requires that the fractional change of δ_{eff} due to the rise of electron temperature should be small [see also remarks following equation (19)]. Thus

$$\frac{\Delta \delta_{eff}}{\delta_{eff}} = \frac{1}{\delta_{eff}} \frac{\partial \delta_{eff}}{\partial T_e} \Delta T_e << 1$$

or

$$\Delta T_e << \left[\partial \ell n \, \delta_{eff} / \partial T_e\right]^{-1} \tag{36}$$

and therefore the eleventh constraint imposes a desirable range of ΔT_e given by

$$\frac{2\,\Delta\,\Phi}{3k n_e \nu_t \delta_{eff}} \ll \Delta T_e \ll \left[\frac{\partial(\ell n\, \delta_{eff})}{\partial T_e}\right]^{-1} \tag{37}$$

The first and second parts of this constraint are compatible except possibly in the rare cases when $\Delta\,\Phi$ and $\partial(\ell n\, \delta_{eff})/\partial T_e$ are both very large. Such cases have yet to be encountered. The first part of this constraint can be incompatible with the seventh constraint and care should be taken if such is the case, to allow for the influence of the terms Φ and $\partial\,\Phi/\partial T_e$ in equations (17) and (18). It should be remembered that with the convention that s_i is positive, the quantity ϵ_i is <u>negative</u> when the electrons <u>gain</u> energy and <u>positive</u> when they <u>lose</u> energy by the processes inherent in $\sum_i s_i \epsilon_i$. Thus when, for example, the electrons gain energy by some process $s_i \epsilon_i$ the values of δ_{eff} calculated from equations (18) to (20) without corrections for the influence of $\partial\,\Phi/\partial T_e$, may be too low.

Observance of these eleven constraints as well as of the conditions leading to equations (16) to (20) is necessary for the design of successful experiments to determine δ_{eff} by this method. It is very fortunate indeed that these constraints and conditions are mutually compatible. Conversely, these constraints and conditions effectively specify the design of the experiment.

There are two additional important relationships that are essential for the design of this experiment. They consist of the expression for ohmic heating $\dot{\Omega}$ of a plasma in the absence of a magnetic field and the appropriate relationship between the electric field E_o and the illumination power P (see Appendix A).

The first of these expressions is given by

$$\dot{\Omega} \equiv \vec{J}_e \cdot \vec{E} = \frac{e^2 n_e \nu_t E_o^2}{2 m_e (\omega^2 + \nu_t^2)} \approx \frac{e^2 n_e \nu_t E_o^2}{2 m_e \omega^2} \text{ when } \omega^2 > \nu_t^2 \tag{38}$$

in watts per m^3, and the second by

$$E_o = (4PZ/A_r)^{1/2} \tag{39}$$

Under the conditions of the experiment (see Appendix A) the impedance Z is close to $Z = 420\,\Omega$ and $A_r = 0.1016 \times 0.1524 = 1.548 \times 10^{-2}\ m^2$ and therefore

$$E_o = (4Z/A_r)^{1/2} P^{1/2} = 330\, P^{1/2} \tag{40}$$

where P is in watts and E_o in V/m.

The operating constraints are summarized in Table I. We can now proceed to define an operating envelope for the experiment.

Operating Conditions

Practical requirements such as the availability and cost of rf power generators, the accessibility of the region within the waveguide, the separation between the waveguide walls that is necessary to admit a plasmajet of several centimeters diameter and the transmission losses associated with ultra high frequencies, resulted in a choice of 2.45 GHz cw for the frequency of the rf power generator. The actual operating envelope for the experiment can now be delineated by making use of the theoretical considerations and constraints, equations (21) to (40), of the previous section. The operating conditions are summarized in Table I.

As soon as the frequency f is specified, we observe from equation (23) that to satisfy the second constraint we must operate the experiment with $n_e < 7.42 \times 10^{15}$ electrons per m^3. To satisfy the first constraint [equation (22), $R_M \geq 25$] for nitrogen with an electron number density $n_e = 7 \times 10^{16}$ and an electron temperature in the jet (independent of n_e) of $T_e = 3600\ ^oK$ (at which temperature $Q_{e,N_2} \approx 9 \times 10^{-20}$ and $\delta_{eff} \approx 5 \times 10^{-4}$) we require $n_{N_2} \geq 1.2 \times 10^{22}$ nitrogen molecules per m^3. Thus if the static temperature in the jet is $300\ ^oK$, we

require a static pressure in the free jet (approximately equal to the pressure in the vacuum tank) of 500 microns (50 newtons/m^2) or less. To satisfy the first constraint ($R_M \geq 25$) for argon with an electron number density $n_e = 7 \times 10^{16}$ and an electron temperature of 3600 ^oK (at which temperature $Q_{e,A} \approx 1.2 \times 10^{-20}$ and $\delta_{eff} = 2.7 \times 10^{-5}$) we require $n_a < 1.6 \times 10^{24}$ argon atoms per m^3. Thus if the static temperature in the free jet is 100 ^oK we require a tank pressure of 22,000 microns or less. Therefore, for strict observance of the first constraint the vacuum tank should be operated at pressures in the range of 100 to 500 microns. However, since we have a quick and easy way of determining the seriousness of any possible deviations from Maxwellian distribution (by observing the linearity of the semilogarithmic plot of the Langmuir probe current-voltage characteristics at low currents) we can probably extend this range up to 1000 microns. Nevertheless, it should be much easier to obtain Maxwellian distributions with argon than with nitrogen (and therefore the semilogarithmic plots of the Langmuir probe characteristics should remain linear over a wider range of bias voltage for argon than for nitrogen).

The third constraint, equation (24), requires that $n_a < 3.4 \times 10^{23}$ for nitrogen at $T_e = 3600\ ^oK$ and $n_a < 2.5 \times 10^{24}$ for argon. These numbers are compatible with the results of our effort to comply with the first constraint, i.e., if we satisfy the first constraint we also satisfy the third.

When a Langmuir probe of 1 mm diameter is used, the fourth constraint, equation (25), requires that the neutral particle density n_a be equal to or less than 10^{22} (corresponding to 400 microns tank pressure at a static temperature of 300 ^oK) for nitrogen and 0.8×10^{23} (corresponding to 1100 microns tank pressure at a static temperature of 100 ^oK) for argon. This constraint also is compatible with the first constraint.

The fifth constraint, equation (26), requires that $n_e >> 5 \times 10^{13}$ and this is compatible with the second constraint, i.e., we can satisfy the second constraint while we also satisfy this constraint.

With $a = 0.1524$ m and $U \leq 3000$ m/sec, the sixth constraint, equation (27), requires that $n_a > 1.2 \times 10^{21}$ for nitrogen (with $T_e = 3600\ ^{o}K$) and $n_a > 9 \times 10^{21}$ for argon (at the same T_e). This constraint is also compatible with the first constraint and implies that the pressure in the vacuum tank should remain above approximately 40 to 100 microns.

The seventh constraint, equation (30), requires that the applied electric field E_o be greater than the minimum electric field required to obtain a minimum elevation of the electron temperature $(\Delta T_e)_{min}$. Now assuming that T_e can be determined within $\pm 100\ ^{o}K$ and that we want the uncertainty in T_e to be of the order of 10%, we conclude that the minimum required electron temperature elevation is $(\Delta T_e)_{min} = 1000\ ^{o}K$. To obtain this elevation at $T_{e1} = T_n$ requires an electric field of approximately 418 V/m (4.18 V/cm) or 1.62 watts of illumination power with N_2 and 99 V/m (0.99 V/cm) or 0.090 watts with argon.

Assuming the initial electron temperature $T_{e, E=0}$ is $2600\ ^{o}K$ while $\Delta T_e = 1000\ ^{o}K$, we obtain $E_p = 795$ V/m for nitrogen and 188 V/m for argon. The eighth constraint, equation (32), requires that $E_o \leq E_p$ and we see that it can be satisfied, if necessary, without much difficulty.

The ninth and tenth constraints are also satisfied when the eighth constraint is satisfied.

A careful estimate of the magnitude of the term $\partial\Phi/\partial T_e$ from the data provided by Allen (ref. 16) and Morris et al. (ref. 17) indicates that the first part of the eleventh constraint, equation (35), is satisfied when $\Delta T_e > 50\ ^{o}K$ for nitrogen and $\Delta T_e > 1000$ to $2000\ ^{o}K$ for argon (depending on the enthalpy). Note that the presence of large concentrations of metastables in the argon jet at certain plasmajet enthalpies may require the operation of the experiment at ΔT_e considerably higher than this lower limit. On the other hand, if the concentration of metastable argon in the jet is somehow suppressed, the required ΔT_e may be considerably lower than this limit. For practical purposes the effect of $\partial\Phi/\partial T_e$ should be investigated in argon experiments by observing the variations of δ_{eff}, as determined by equations (19) or (20), with plasmajet enthalpy and

applied ΔT_e (or illumination power) and care should be taken to carry out the measurements in a region where the variation of δ_{eff} with these two parameters is negligible.

An estimate of the magnitude of the term $\partial(\ell n\, \delta_{eff})/\partial T_e$ from the room-temperature data of Crompton and Sutton for nitrogen (ref. 18) shows that even at $T_e \approx 11,000\ ^oK$ (where δ_{eff} begins to vary rapidly with T_e) the magnitude of this derivative is such that $[\partial(\ell n\, \delta_{eff})/\partial T_e]^{-1} \approx \delta_{eff}\, \Delta T_e/\Delta \delta_{eff} \approx 2200\ ^oK$ and therefore an elevation of the electron temperature by any amount less than 2200 ^oK will satisfy the second part of the eleventh constraint, equation (36), since provided we operate below $T_e = 11,000\ ^oK$ (say, at less than 10,000 ^oK) any elevation by an amount less than 2200 ^oK will automatically be much less than $\partial T_e/\partial(\ell n\, \delta_{eff})$ evaluated at $T_e < 11,000\ ^oK$ ($\Delta T_e/\Delta \delta_{eff}$ decreases rapidly at $T_e \geq 11,000$). Therefore, for nitrogen we can write for the required electron temperature elevation, $\Delta T_{e,req}$

$$50\ ^oK < \Delta T_{e,req} < 2200\ ^oK, \quad \text{for } N_2,\ T_e < 10,000\ ^oK$$

where the "much smaller than" requirement of equation (36) has been relaxed since the term $\delta_{eff}\Delta T_e/\Delta \delta_{eff}$ is considerably larger than 2200 ^oK at $T_e < 10,000\ ^oK$. For argon, by definition, $\delta_{eff} = \delta_{el}$ is constant with T_e and therefore the second part of the eleventh constraint is always satisfied. The electron temperature elevation required for determination of fine structure in $\delta_{eff} = \delta_{eff}(T_e)$ for argon is therefore primarily dependent on the magnitude of the masking effects due to $\partial\Phi/\partial T_e$. These effects can be kept small when

$$\Delta T_{e,req} > 1000 \text{ to } 2000\ ^oK, \quad \text{for A},\ T_e < 7,000\ ^oK$$

It should be noted that, for $\omega = 1.54 \times 10^{10}$ rad/sec, the ohmic heating term given by equation (38) becomes, with the aid of (40),

$$\dot{\Omega} = 5.93 \times 10^{-29} n_e \nu_t E_o^2 = 6.42 \times 10^{-24} n_e \nu_t P \qquad (41)$$

At T_e = 3600 ^{o}K and the conditions imposed by the first and second constraints, we obtain

$$\dot{\Omega} = 1.81 \times 10^{-4} P, \quad W/cm^3, \quad \text{for } N_2$$

and (using typical momentum cross-sections for argon given by reference 19)

$$\dot{\Omega} = 3.22 \times 10^{-3} P, \quad W/cm^3, \quad \text{for A}.$$

We observe from these values of $\dot{\Omega}$ and the power requirements of the seventh and eighth constraints that the increase in gas enthalpy due to ohmic heating of the electrons will indeed be small even if we assume instantaneous electron energy relaxation.

Experimental Apparatus

Vacuum tank. - The experiments are carried out in a 4-foot (1.22 m) diameter, 10-foot (3.05 m) long stainless-steel vacuum tank with the arcjet mounted on the 4-foot diameter access door that also serves as the front bulkhead or closure. The axis of the arcjet is at the center of the door and coincides with the axis of the tank. The primary vacuum system consists of a Rootes-type dry blower (Stokes Model 1722-S Mechanical Booster Type high-vacuum pump with 1600 cfm maximum displacement and an ultimate blank-off pressure of below 2×10^{-4} torr, driven by a 10 hp open motor) backed-up by a Stokes Microvac Model 412-H water-cooled rotary-piston mechanical high-vacuum fore pump (with 300 cfm displacement, driven by another 10 hp motor). Both of these pumps were manufactured by the Stokes Equipment Division of Pennsalt Chemical Corporation. With this vacuum system the tank can reach a pressure of 1 micron in less than 20 minutes of pumping time. The tank is equipped with an 8-inch high-vacuum gate valve that can be used to throttle the vacuum pumps and a 1-inch ball valve that can be used to bleed air into the tank. The tank is connected to the vacuum system through an 8-inch diameter flexible bellows.

The tank is equipped with five 12-inch portholes and one 6-inch porthole that serve either as viewports or provide convenient locations for feedthroughs for the various gas-, power-, and water-lines that are connected to apparatus inside the tank. The space between the front and rear 3-foot-high legs of the tank is filled with a one-foot deep slab of concrete. This slab weighs in excess of 4000 lbs and was poured around several large bolts set into the concrete floor. It has proved effective in reducing the transmission of vibrations from the vacuum system to the tank and the equipment in it.

Arcjet system. - The arcjet system consists of a Thermal Dynamics Corporation 50N torch provided with a 0.65-inch long, 0.625-inch diameter plenum chamber downstream of the arc. The plenum chamber exhausts into the vacuum tank through a conical supersonic nozzle of 8° 30' half-angle with a throat diameter of 0.165 inches and an exit diameter of 0.500 inches. The diameter of the hole in the anode insert used with this nozzle is 0.188 inches. For lower flow rates (less than 0.5 gm/sec) a supersonic nozzle of the same half-angle but a throat diameter of 0.091 inches and an exit diameter of 0.425 inches can be used. The anode insert diameter for this nozzle is 0.100 inches. This arcjet is powered by three TDB1A-14 selenium rectifiers manufactured by the Miller Electric Manufacturing Co. Each of these rectifiers is rated at 14 kW on a continuous duty cycle and 20 kW maximum output.

The primary gas is injected into the arc chamber of the arcjet. A secondary gas can be injected into the plenum chamber. The primary and secondary gases are metered through calibrated tapered-glass-tube meters. Up to four different separately-metered gases can be mixed in any desirable proportions before injected into the primary or secondary gas feed lines. Four Simet Proportional Mixers (each consisting of a throttling valve and a flow meter and made by National Welding Co.) are used for the injection of these additive gases. Besides the primary and secondary flow meters the arcjet control console is equipped with a voltmeter, an ammeter, primary and secondary gas flowmeter pressure gauges, hf arcjet starter, off-and-on control, arcjet power control, water

coolant flow meter and water coolant entry and exit thermometers. The primary and secondary gas temperatures are measured by additional thermometers placed upstream of the gas flow meters.

This arcjet can easily attain enthalpies of up to 40 MJ/kg (17, 200 BTU/lb) and stagnation temperatures of approximately 8, 000 ^{o}K with nitrogen at plenum chamber pressures (stagnation pressures) in the vicinity of 1 atmosphere. It can attain considerably higher stagnation temperatures with argon or helium (approximately 14, 000 ^{o}K). The manufacturer (Thermal Dynamics Corporation) claims that it is possible to attain enthalpies up to 260 MJ/kg (60, 000 BTU/lb) with nitrogen (with corresponding stagnation temperatures between 10, 000 and 14, 500 ^{o}K indicating that the stagnation pressure ranges between 4×10^{-4} and 2×10^{-1} atmospheres) and stagnation temperatures up to 28, 000 ^{o}K with argon and helium. Under the usual operating conditions the arcjet chamber pressure is in the range of 0. 1 to 1 atm with nitrogen and 0. 5 to 2. 5 atm with argon.

Microwave illumination system. - A schematic of the microwave system used to make the necessary measurements is shown in figure 1. The Raytheon Corporation rf power generator is stable when operating above 10 watts cw and for this reason, rather than operate the unit at very low power levels, an attenuator consisting of a long coaxial cable in series with a variable attenuator is used to give stable operation in the lower ranges of illumination power. Figure 2 is a schematic of the special waveguide, designed to illuminate the plasma on the basis of the calculations given in Appendix A. The electric field in this waveguide test section has been measured with a carefully calibrated search coil (traversed down the centerline of the waveguide, i. e., the x-axis) and both its magnitude and distribution have been found to correspond almost exactly to the theoretically predicted field that one expects for a TE_{10} dominant mode (see Appendix A). Since the experimentally determined E_o was smaller by 15% or less from the theoretically predicted value of E_o while all the assumptions made in reducing the experimental data on the determination of E_o were such that they are expected to lead to slightly smaller values

of E_o, the theoretical value of the electric field given by equations (39) and (40), was used in interpreting all experiments.

The microwave illumination system is equipped for measuring (a) the power fed into the waveguide, (b) the power leaving the waveguide and (c) the power reflected from the waveguide. Since the waveguide and associated connector losses were found to be symmetric, i.e., they were the same no matter from which end of the waveguide the power entered, the illumination power P is determined by summing the input and output power and dividing by two. Usually the illumination power is 80% to 90% of the power input to the waveguide.

Measurements of the reflected power are carried out to ensure that reflection is negligible (and therefore the second constraint is observed) and that the insertion of the Langmuir probe produces negligible or no interactions with the rf field in the waveguide.

Langmuir probe system and traversing mechanism. - Electron temperature measurements are carried out with 0.2 and 1-mm-diameter cylindrical Langmuir probes. These consist of a tungsten wire of the same diameter inserted through a quartz capillary tube with O.D. of approximately 0.5 to 0.7 cm and I.D. slightly larger than the O.D. of the wire. The front end of the quartz tubes is given a conical shape of approximately 30° half-angle and the tungsten wire is pulled through a hole at the center so that it protrudes the desired length ahead of the cone (5 to 7 mm for the 1 mm diameter wire). At the lower enthalpies (less than 20 MJ/kg) these probes are effectively cooled by radiation and so far they have never melted, thanks to the low pressures in the vacuum tank that decrease the heat transfer rate and the enthalpy flux. The tungsten wire is long enough to reach outside the tank through a special rubber-and-vacuum-grease seal. Since the distance from the probe tip to the seal is approximately 8 feet, the wire at the seal is never significantly above room temperature.

A gas-cooled probe was also designed and tested for operation at higher enthalpies. This probe consists of an outer jacket made of a seamless tube of 90% platinum-10% iridium with an outside diameter of 0.050" (1.25 mm) and a wall thickness of 0.007", over an inner

hypodermic 304-stainless steel tube with an outside diameter of 0.028" and a wall thickness of 0.004". The outer Pt-Ir jacket is joined to an outer 0.187" O.D. 304-stainless steel tube, of 0.022" wall thickness, through a flare adaptor. The flare adaptor is soldered to the stainless outer tube and the platinum jacket of the probe with Easy Flow 45 solder. Inside the 0.187" O.D. outer tube is a 0.125" O.D. 304-stainless steel tube that is soldered to the inner hypodermic 0.028" O.D. tube of the probe. The coolant gas comes in, flows through the 0.125" tube, squirts through the end of the 0.028" hypodermic against the front closure of the Pt-Ir jacket and returns through the space between the hypodermic and the jacket and between the 0.125" and 0.187" tubes and finally through a hose connected to a feedthrough at the vacuum tank wall, to be exhausted outside the tank. The gas is supplied, at 400 lb/in^2, to the 0.125" O.D. inner tube through a high-pressure hose connected by means of another feedthrough to a compressed-nitrogen cylinder outside the vacuum tank. All connections and feedthroughs are carefully tested for leaks before each experiment. The 0.187" O.D. tube is inserted into a 0.7 mm O.D. quartz tube whose tip is tapered so that it fits closely around the 0.050" O.D. probe which protrudes 7 mm beyond the quartz.

Although some initially promising results were obtained with this probe, it failed, for reasons as yet undetermined, at the point where the Easy Flow solder joins the platinum tube to the flare adaptor that connects the platinum probe to the outer 0.187" O.D. stainless tube.

The Langmuir probe is mounted on a three-degree of freedom traversing mechanism. The traversing mechanism rides on two 9-foot-long 1-1/4" square, hollow cross-section, stainless-steel rails, water cooled, that are mounted firmly on the right and left walls of the tank parallel to the tank axis and about 3 feet from the bottom of the tank.

An outer carriage rides on eight ball-bearing rollers that ride backward and forward on the rails to provide traversing in the flow direction (x-axis of figure 1). The outer carriage contains two more rails, approximately 30" long, mounted in such a way as to provide traversing in the right-and-left direction (z-axis of figure 1). An inner carriage

rides on these rails and contains a worm-screw gear and two stabilizing rails for up-and-down motion of the traversing platform. Mounted on this platform is a round heat-exchanger and coaxial with the heat-exchanger and through a small hole at the center of its backplate is mounted the 22-inch-long quartz probe shield surrounding the stem of the probe. The Langmuir probe usually protrudes about 15 to 18 inches in front of the backplate of the heat-exchanger. The end of the quartz probe shield is usually 4 to 7 inches behind the heat-exchanger backplate and is therefore completely shielded from the hot gases.

The length of the quartz tubes that form the outer shield of the stem of the probe is 22 inches.

Back-and-forth motion (x-axis) is provided by continuous wire belts attached to both sides of the outer carriage parallel to the rails and driven by a high-vacuum-rated electric motor mounted inside the vacuum tank. Right-and-left motion (z-axis) is provided by a similar drive mechanism mounted on the outer carriage. Up-and-down motion (y-axis) is provided by a high-vacuum-rated electric motor that drives the worm-screw. The position is sensed by Selsyn motors (motion and position transmitters and receivers) and Veeder-Root counters (position displays). Thus only electrical power lines enter into the vacuum tank to actuate and readout the traversing mechanism. The absolute accuracy of this system is ± 0.005" and tank warping is thought to be the limiting factor.

The heat-exchanger is so efficient in removing the energy from the gas that neither the tank walls nor the pump inlet experience a temperature that rises significantly above room temperature.

The Langmuir probe and the heat-exchanger are rigidly mounted together and move simultaneously and predictably so as to traverse approximately 6 feet along the length of the tank (x-axis or flow direction) approximately twenty-four inches right-and-left (z-axis) and sixteen inches up-and-down (y-axis). The position displays and traverse controls are mounted in a control panel outside the tank.

The electrical circuit for the Langmuir probe is substantially the same as used by Kelly et al. (ref. 12) except that their 100 Ω resistor, which is used as a shunt to measure the current, is replaced in our apparatus by a high-precision (better than +0.5% of full scale) decade capable of varying the value of this resistance from 1 to 99,999 Ω. The maximum bias voltage for the probe is 24 volts (supplied by four dry cell batteries, such as Eveready 510S, connected in series, each battery made up of four size F cells). A four-position switch is provided that gives zero bias (off position), full positive bias (zero to +24 volts), negative and positive bias (-12 to +12 volts) and full negative bias (zero to -24 volts) on the probe. The probe bias in each switch position is varied by a coarse sweep (provided by a one-turn dual pot with 25,000 Ω in each section rated at 2 watts for each section, the two sections series-connected for a total of 4 watts) and a fine sweep (provided by a one-turn potentiometer with a resistance of 5000 ohms and a rating of 4 watts). Ten-turn pots were also used for these sweeps but after some experience was obtained they were replaced by the simpler pots. As the potentiometer sweeps the bias voltage on the probe, it is recorded on the x-axis of an x-y recorder (Models 135-A or 7000-A, Moseley Division of Hewlett-Packard Corp.) which also records the voltage drop acrss the decade (usually set at 100 Ω) on the y-axis, to obtain the current-voltage characteristics of the Langmuir probe.

Probe noise spectrum analyzer and integrating readout. - As a preliminary step towards developing an automated noise-suppressing electron-temperature (ANSET) readout system a Hewlett-Packard 3460 integrating voltmeter with 0.1 sec maximum integrating time was used to make a preliminary analysis of the noise spectrum of the Langmuir probe operating in a nitrogen plasma in order to decide (a) if the noise is truly random and can be averaged or integrated out and (b) what is the optimum averaging time for improved signal-to-noise ratio. The results of more than 100 different readings at each of several probe bias voltages were plotted as an integral spectrum and the RMS noise and percentage noise were obtained. It was concluded that (a) the major source of noise

seems to have Gaussian distribution, (b) an averaging time of 10 seconds would ensure that probe currents can be measured to the order of better than 1% of their value at any probe bias setting, (c) the RMS noise current seems to be roughly proportional to the square root of the electron current, and at the highest electron current, where the RMS error is about 4%, one can make a model of the electron current coming in bursts and calculate that the bursts' frequency should be about 6 kHz. An examination of the probe current by a fast oscilloscope indicated that, under some arcjet operating conditions, current bursts do indeed appear to be coming at about this frequency.

That the source (arcjet) is stable for 10-second intervals was shown by using an x-y plotter to obtain time recordings of the current to the probe at several bias voltage settings. During the course of these measurements it was discovered that there seems to exist a long-term drift in the arcjet current and voltage charcteristics that causes the probe potential to drift or change. These drifts show up as a sudden (i.e., in less than 0.1 sec) drop of the arcjet voltage by 1 to 3 volts followed by a slow but accelerating drift of the voltage to approximately its original value. The period of this drift is usually of the order of 10 minutes. While this drift occurs the probe characteristics also drift (i.e., are displaced) on the bias voltage axis without a change of the shape or slope of the curve.

The results of these studies indicate that this arcjet can operate in two distinct modes: The "noisy arc" mode (where all evidence points to an intermittent arc that strikes and is extinguished with a period of the order of 100 μ sec) and the "quiet arc" mode (where the arc operates continuously while the plasma and the probe signal are quiet). This quiet arc mode is encountered when the arc chamber pressure is of the order of 0.15 atmos absolute (in nitrogen). The probe then is so quiet that the noise is negligible. Drifts occur with much lower frequency when the arc operates in the "quiet" mode. However, not all operating conditions and requirements can be satisfied by arcjet operation in the quiet mode and the effort to develop an integrating probe readout that enhances the signal-to-noise ratio was continued.

As a preliminary step, before employing digital integrators in the ANSET readout system, it was decided to extend the linearity of the Langmuir probe current-voltage plots by a full decade by surveying very accurately the region close to 0 volts (i.e., to establish the linearity down to the 0.1 mv/inch range of the recorder whereas previously it was limited to 1 mv/inch). The probe resistance remained at 100 Ω. Data were taken, based on a less accurate integration procedure as follows: an automatic voltage stepper was built and was connected to two x-y recorders, one of which plotted "voltage applied"(in steps) vs "time", and the other plotted the corresponding "probe current" (voltage developed across a 100 ohm series resistor) vs "time". By a procedure of visual integration of the graphs, the above technique allows a fairly accurate estimate of the expected value (mean) of the stochastic process describing the current through the probe. Since the power-density spectrum of the noise was found to have all components in the range of 10 Hz to 10 kHz, it was concluded that an integrating time of 5 sec per voltage-step is long enough to minimize the noise effect, and short enough to keep drift from becoming a problem.

The automatic-voltage stepper's versatility also permits us to concentrate on the most critical region of the graphs and to specify accurately the values of the coordinates there, by essentially magnifying this region ten-fold.

Repeated measurements of δ_{N_2} with this technique yielded values very close to those previously reported, as was to be expected since the "integrating" was again done by the x-y plotter and the human eye. Nevertheless, the linearity of the probe characteristics was extended over an additional decade and useful measurements of δ_{N_2} could be obtained in the presence of considerably higher noise levels.

The automatic voltage stepper (AVS), is fast and uses integrated circuits, of the type used in the newest digital computers, throughout. Timing is controlled by an extremely accurate, temperature controlled 100 kHz crystal oscillator employing unijunction semiconductors. Front-panel controls allow starting and stopping the sequence of steps at any time, as well as monitoring the progress of the sequences. The AVS is

only one of the four main components of the ANSET readout system. The other components consist of a Hewlett-Packard 2401C integrating digital voltmeter, the logic circuits coupling the output of the integrating voltmeter to a coder (card, paper or tape punch) and the computer and computer program that convert the coded data into an electron temperature.

Testing of this ANSET readout system is incomplete. From the available data it appears that the accuracy of this or similar fast and sophisticated digital integration equipment is really necessary before the question of the influence of noise on the measurements is given a final and authoritative answer.

The spectroscopic apparatus used to determine the energy state of the hot gas by observation of the spectral intensity of the radiation emitted from the plasma when it is excited by an electron beam, is described in the next section.

ENERGY STATE OF THE GAS

To define the energy state of the hot gas of these experiments, an electron beam device was built and used to ionize and excite directly rotational and vibrational bands of diatomic components of the plasma. The rotational and vibrational fine structure of the spectrum of the radiation emitted from the molecules ionized by the beam was then used to determine the rotational and vibrational temperatures of these moledules.

Spectroscopic analysis of the radiation emitted when a gas is excited by an electron beam has been used by several investigators (e. g., Muntz and Marsden, reference 20, Petrie, references 21 and 22, and Sebacher, reference 23) to define the energy state of vibrationally and rotationally relaxing high-speed flows of nitrogen and other gases.

The electron beam diagnostic technique is particularly attractive because (a) the small beam diameter (typically 1 mm) and small beam-spreading leads to good spatial resolution and requires no symmetry (axial or otherwise) of the plasma jet in order to obtain distributions of

the observable plasma parameters and (b) it has no measurable influence on the basic energy state of the test gas and can be applied to any low-density flow regardless of the gasdynamic, chemical and thermodynamic nature of the gas. In this technique, described in detail by other authors (refs. 20 to 24), the narrow beam of electrons is projected across the flow and the interaction of the electrons with gas particles produces a thin column of radiating gas that is nearly coincident with the beam. In air or nitrogen the emission is excited by collisions between beam electrons and nitrogen molecules in the ground electronic state $(N_2 X^1\Sigma)$. In specifying the detailed mathematical model for analysis and interpretation of the observed radiation, it is assumed that (1) excitation occurs directly from the N_2 ground state to the $N_2^+ B^2\Sigma$ state of the nitrogen ion, (2) the Franck-Condon principle applies directly in the excitation process and a spontaneous radiative transition of the excited ion to its ground electronic state $(N_2^+ X^2\Sigma)$ occurs before any collisional process takes place, (3) Born's approximation holds (since the energy of the beam electron is large compared to the ionization energy of N_2) and the rotational excitation process obeys the usual optical selection rules (i.e., the probabilities of transition between the rotational energy levels are assumed equal to the corresponding values for the usual optical transitions) and (4) an expression for the population in the N_2 ground state is available (in this case Boltzmann population distributions for the rotational and vibrational temperatures, references 25 and 26). Previous analyses (refs. 20 to 24) substantiate the validity of the assumed excitation process under special conditions. Similar conditions that justify these assumptions also prevail in our experiments and therefore the rotational and vibrational temperatures determined by this technique are those of the un-ionized nitrogen molecules in the ground electronic state, i.e., the corresponding temperatures of the molecules before excitation by the electron beam.

When an electron beam with energies in the range of 10 to 30 Kev is passed through air or molecular nitrogen, the predominant radiation is due to the first negative emission system of N_2^+. The most intense band in the emission is the (0, 0) band at 3914 Å. Radiation has also been

observed from bands in the (0, 2), (0, 1) and (1, 0) progressions. In addition, bands from the second positive system of N_2 have been observed with intensities near that of the N_2^+ (1, 0) band.

The rotational temperature of N_2 is determined by measuring the relative emission intensities of the rotational lines in any given N_2^+ band [usually the (0, 0) band at 3914 Å]. The N_2^+ bands consist of a R-branch and a P-branch of rotational lines. The P-branch lines are very close together and form the band head. The R-branch lines are spaced rather evenly towards the violet with increasing rotational quantum number values and can be resolved by a spectrograph with moderately good resolution. The rotational temperature is obtained from the measurement of the intensities of the R-branch lines by the straight-line plot method discussed in the literature (refs. 20 - 24). The accuracy of this determination of the rotational temperature depends on the sensitivity of the optical system used (i.e., on the signal-to-noise ratio) and it appears that it is probably limited to ± 1% or less even for a system of moderate sensitivity and resolution. Such a system can be expected to achieve a practical accuracy of ± 3% in the determination of rotational temperatures by these techniques (refs. 20 - 24).

The vibrational temperature is obtained from the measurement of the integrated emission intensities of at least two vibrational bands. The bands in both the (0, 2) and (0, 1) progressions of the first negative emission system of N_2^+ are suitable for vibrational temperature measurements. The (0, 1) progression has intensity peaks at 4278 Å for the (0, 1) band, at 4236 Å for (1, 2), at 4199 Å for (2, 3) and at 4167 Å for the (3, 4) band. The (1, 0) progression is overlapped by the (0, 1) progression of the N_2 second positive system. Since the Franck-Condon factors and wavenumbers of the bands are known, a measured integrated intensity ratio, e.g., between the (0, 1) and (1, 2) bands or the (0, 1) and (2, 3) bands, can be used to obtain the magnitude of the vibrational temperature. The accuracy of this vibrational temperature determination depends mainly on the technique employed for intensity measurement; however, uncertainties in the Franck-Condon factors and errors associated with the integration of

the band intensities probably limit the accuracy of this temperature determination to approximately ±6%. A system of moderate sensitivity and resolution can be expected to achieve a practical accuracy of ±9% (refs. 20 - 24).

Such an optical system, consisting of a Jarrell-Ash 0.5-meter Ebert scanning spectrometer and an EMI 9502S photomultiplier tube, was built and used to obtain rotational and vibrational temperatures in the nitrogen plasmas previously described (ref. 1). The spectrometer used a grating with 1180 grooves/mm blazed for 4000 Å. The effective aperture ratio of the spectrometer was f/8.6 and the resolution was at least 0.2 Å in the first order. Typical dark current of the photomultiplier was 0.5 nanoamps. The photomultiplier signal was processed by a Keithley Instruments Model 417 picoammeter and recorded by a Moseley 7000A x-y recorder synchronized with the scanning drive of the spectrometer. A separation of approximately 1 cm between the peaks of the Hg 3131 Å doublet (3131.55 Å and 3131.83 Å) was easily obtained by the recorder. When it was deemed necessary to eliminate or check the drift in the electron beam intensity or other sources of noise, zero-shift or poor response, as well as the effect of integrated noise, a light beam splitter was used to divert part of the light beam to another photomultiplier (RCA 1P28). This reference photomultiplier was used to monitor total radiation intensity of selected parts of the spectrum (by means of selected light filters) while scanning (e.g., total intensity of the (0, 0) band) and its signal was also processed by a Keithley 417 picoammeter. The electrical signal from the spectrometer photomultiplier (EMI 9502S) was divided by the signal from the reference photomultiplier by an on-line analog computer (Electronic Associates TR-20, 1967 model). This division eliminates the effects of gradual changes in beam current which might occur during a scan as well as other sources of possible error due to time-dependent fluctuations in light intensity. The Keithley 417 picoammeters proved particularly convenient because they include a bucking network so that d.c. noise can be eliminated. For calibration of the optical system a standard of spectral irradiance traceable to the National Bureau of Standards (coiled-coil

tungsten filament quartz-iodine lamp calibrated over the spectral range from 2500 Å to 25,000 Å) with a special power supply was obtained from Eppley Laboratory, Inc.

The spectrometer light-gathering system had an effective aperture ratio of f/4. The spectrometer slit image was focused on the space occupied by the electron beam by backlighting. The image was approximately 1 mm high. Therefore the volume of radiating plasma examined by the spectrometer is of the order of 1 mm cubed. The electron beam was at right angles to the plasmajet axis and shooting down from the top. The spectroscope axis was at right angles to the electron beam axis on the left-hand side of the plasmajet axis and almost perpendicular to it. (The angle between the optical axis and the perpendicular to the plasmajet axis was 6.5°). An observation port was on the right-hand side of the plasmajet axis. The cylindrical Langmuir probe was on the plasmajet axis (pointing upstream) at approximately the same distance from the arcjet nozzle exit plane as the electron beam (approximately 16 cm). For the electron beam experiments the Langmuir probe was moved 15 cm further downstream and the microwave apparatus was removed from the vacuum tank.

For these measurements, the arcjet was operated at an energy input to the gas of between 2×10^6 and 4×10^6 joules/kg and the stagnation pressure in the plenum chamber varied from 0.5 to 0.6 atmospheres, corresponding to the conditions of reference 1.

Table II shows typical vibrational and rotational temperatures, T_{vib} and T_{rot} respectively, measured with this apparatus in a pure nitrogen plasma. Table II also shows the corresponding free electron temperatures $T_{e,E=0}$ (at zero rf illumination power and with the electron beam off) obtained with the Langmuir probe, the corresponding stagnation temperature T_o obtained from the average enthalpy derived from an arcjet energy balance, and the corresponding static temperature T computed from an isentropic expansion from the stagnation pressure and temperature to the vacuum tank pressure of 400 microns. It is seen that $T_{e,E=0}$ is in substantial agreement with the measured vibrational temperature and T_{rot} is in substantial agreement with T. The

implications of these measurements are that under the conditions of the experiment the electron temperature is closely coupled and in near equilibrium with the vibrational temperature even for pure nitrogen, as previously suspected (ref. 1). In addition, the rotational temperature appears to be closely coupled to the static (translational) temperature as expected for these conditions (refs. 20 - 24).

Now consider the case of thermal equilibrium between the various degrees of freedom of the molecule, under conditions such that the radiative loss term $\dot{R}$ and the secondary energy exchange term $\sum_i s_i \epsilon_i$ are both negligible. Then the contributions to the energy loss factor from the various excitation mechanisms (i.e., elastic or translational, rotational, and vibrational) can be simply added to yield the total inelastic energy loss factor, δ_κ or δ_{eff}. Moreover it can be shown that under certain reasonable assumptions each of these contributions δ_j, becomes independent of the associated excitation temperature T_j^* of the molecule when this temperature is much larger than the characteristic temperature θ_j for that process, i.e., the contribution δ_j is independent of T_j^* for $T_j^* >> \theta_j$ and $T_e >> \theta_j$. For example, the contributions to δ_κ from vibrational excitation, δ_v, becomes

$$\delta_v = \frac{2}{3} P_{1,0}(T_e) \cdot (1 - e^{-\theta_v/T_e}) \left[\theta_v/(e^{\theta_v/T_e} - 1) - \theta_v/(e^{\theta_v/T_{vib}} - 1) \right] \times$$

$$\times (T_e - T_{vib})^{-1} \qquad (42)$$

where $P_{1,0}(T_e)$ is the de-excitation probability for the first excited vibrational state by electron collisions, θ_v is the characteristic temperature for vibrational excitation and $T_{vib} = T_j^*$ is the vibrational temperature. *

* Equation (42) can be obtained by specializing the theory of translational-vibrational relaxation as outlined by Montroll, E. W.; and Shuler, K. E.: J. Chem. Phys. 26, (1957) p. 454, to the case of electrons as collision

It is easily seen from equation (42) that when $T_{vib} >> \theta_v$ and $T_e >> \theta_v$, δ_v is independent of T_{vib} . Similar arguments can be made for the other excitation processes. At the same time δ_j is negligible when $T_e << \theta_j$ and $T_j^* << \theta_j$. When the gas is not at equilibrium each δ_j is computed at the temperature T_j^* (ref. 3). Therefore, for the gases and in the range of temperatures of interest to us (roughly 300 ^{o}K to 10, 000 ^{o}K) the contribution to δ_κ or δ_{eff} from rotational excitation energy loss mechanisms is substantially independent of the rotational temperature and only the contributions from vibrational and electronic excitation are dependent on the associated excitation temperatures T_{vib} and T_{elec} . Similarly for the gases and conditions of interest to us, $\dot{R}$ and $\sum_i s_i \epsilon_i$ can be considered negligible.

This is a consequence of the fact that θ_{rot} is 2. 87 ^{o}K for N_2, 2. 08 ^{o}K for O_2 and 2. 45 ^{o}K for NO while θ_v is 3392 ^{o}K for N_2, 2273 ^{o}K for O_2 and 2738 ^{o}K for NO and θ_{elec} is 71584 ^{o}K for N_2, 11392 ^{o}K for O_2 and 174 ^{o}K for NO (ref. 27). In other words, in this range of temperatures, if we have N_2 , O_2 or a mixture of the two, excluding nitric oxide, at equilibrium at some gas temperature $T_g = T_{rot} = T_{vib} = T_{trans} =$ etc., this gas, to good approximation, will have the same energy loss factor as a gas with the same vibrational temperature $T_g = T_{vib}$ but different rotational and translational temperatures, assuming that $T_{rot} >> \theta_{rot}$ and that the vibrational and electronic excitation are at equilibrium at the same temperature (or that the contribution to the energy loss factor by electronic excitation is negligible). Since the characteristic temperature for electronic excitation for N_2 is high, the contribution to the electron energy balance due to electronic excitation is negligible in the temperature range of interest and, in this range,

---

partners. The assumptions made in this derivation are: (1) ideal harmonic oscillator behavior of the diatomic molecules, (2) the Landau-Teller approximation for the collisional transition probabilities [Landau, L. ; and Teller, E. : Physik. Z. Sowjetunion 10, (1936) p. 34], (3) the existence of a Boltzmann distribution for both the population of the vibrational states and for the energy of the free electrons.

knowledge of the variation of δ_{N_2} with vibrational temperature is sufficient to determine the influence of gas temperature on δ_{N_2} (always provided T_{rot} is much greater than θ_{rot}). In other words, vibrationally hot N_2 is al , simply hot as far as δ_{N_2} is concerned. The same statements can also be made for oxygen, at least in the lower half of the temperature range of interest (and in the upper half dissociation begins to make the question academic).

Therefore, for nitrogen, oxygen or any N_2-O_2 mixtures (that somehow are prevented from containing NO) at equilibrium at any temperature T_g in the range from approximately 300 ^{o}K to 10, 000 ^{o}K, the electron energy loss factor is the same as the electron energy loss factor of the same mixtures at a vibrational temperature $T_{vib} = T_g$ in the same range but not at equilibrium, provided the rotational temperature is at least 200 - 300 ^{o}K. We see from table II that this condition is met in our experiments and therefore T_{vib}, which turns out to be essentially equal to $T_{e, E=0}$ in this work, is sufficient to characterize the effective temperature T_g of the nitrogen gas as far as the electron energy-loss factor is concerned.

The situation is not necessarily the same for other gases. For example, with monatomic gases it follows from the definition of δ_{eff} that the translational temperature should be sufficient to characterize the energy state or effective temperature T_g of the gas as far as δ_{eff} is concerned.

EXPERIMENTAL RESULTS

Experiments were carried out to measure the electron temperature as a function of the power input to the cell, in order to obtain dP/dT_e in argon, nitrogen and nitrogen-oxygen mixtures preheated by the arcjet. In all these experiments the reflected rf power was negligible and there was no observable interaction between the Langmuir probe and the microwave cavity or the rf power (e. g., the reflected power did not change when the probe was withdrawn from the cavity). The ohmic heating power

loss $\dot{\Omega}$ was also negligible compared to the illumination power per unit volume of plasma.

As far as could be determined, the species concentrations at the probe were not at equilibrium with T_g, or with $T_{e,E=0}$, or with an easily identifiable excitation temperature of the gas T^*, or with the electron temperature after the application of rf power, or with the stagnation temperature of the gas in the plenum chamber, T_o, as determined from an average enthalpy derived from an arcjet energy balance. All evidence pointed to the existence of an arc temperature $T_{arc} > T_o$ which was responsible for the species present originally in the arc chamber.

Typically, in these experiments the particle concentrations were $n_e \approx 10^{16}$ electrons/m^3 or slightly larger and $n_a \approx 10^{22}$ atoms or molecules per m^3. The electron concentrations were obtained by the Langmuir probes and the neutral particle concentrations from the pressure in the tank and the static temperature in the jet. Note again, however, that in accord with equation (20) these measurements are not required to find the energy loss factor. They serve to define the range of experimental conditions and to verify that the constraints listed earlier are in fact satisfied.

Experiments with Argon

For the argon experiments, the appropriate gas temperature T_κ o $T_{\kappa,s}$ for equations (4) or (8) is the temperature that describes the average energy (excluding electronic excitation with the associated temperature, T_{elec}) of the atoms and is identical to the static temperature T of the gas. In a simple gas, consisting of one heavy component, δ_{eff} is of course equal to the energy loss factor δ_κ of that gas. Choosing the reference temperature T_n to be the gas temperature T_g, which is identical with T in this case, we can use equations (7) or (9) to define $\delta_\kappa = \delta_{eff} = \delta_A$ for argon. Then we can use the appropriate expression among equations (17) to (20) to determine δ_A from the experimental data.

When this experiment was carried out with argon under conditions such (ref. 28) that the electron temperature at the probe with zero applied electric field, $T_{e, E=0}$, was equal to the excitation temperature $T^* \equiv T_{elec}$ of the argon atoms and was in the range $2100\ ^{o}K < T_{e, E=0} < 3400\ ^{o}K$, it was found, by using the second half of equation (20) in a simplified form given by

$$\delta_{eff} = 2.86 \times 10^{-6} \left(\frac{4Z}{A_r}\right) \left(\frac{\Delta P}{\Delta T_e}\right) = 0.312 \frac{P}{T_e - T_{e, E=0}} \qquad (43)$$

that the computed energy-loss factor was approximately 13% higher, at $\delta_{eff} = 3.10 \times 10^{-5}$, than the elastic energy-loss factor for argon, $\delta_{A, el} = 2.73 \times 10^{-5}$. Since the enthalpy of the argon in these experiments was in the range of 10^6 joules/kg to 2×10^6 joules/kg, while the static temperature $T = T_g = T_{tr}$ of the gas was in the range of 100 to 200 ^{o}K, it appears unlikely that this discrepancy was due to radiation or other losses. It is much more likely that the electric field in the waveguide (or the illumination power applied to the plasma) is overestimated by this amount. The results of the measurement of the waveguide electric field, discussed in the section on experimental apparatus, appear to confirm this view.

Typical results with argon at these low enthalpies are summarized in table III. The stagnation temperature of the argon was in the range of 2000 to 3500 ^{o}K. The results of table III are obtained by making use of equation (43). There is clear evidence (ref. 1) that at higher electron temperatures $T_{e, E=0}$, the energy-loss factor for argon as computed from equation (43) is larger than the elastic energy-loss factor. This result indicates that some inelastic process or processes serve as a sink of the electron energy in argon and that these processes significantly influence the determination of δ_{eff} by equation (43) due to the smallness of δ_{eff} and of the term $(3/2)\, k n_e \nu_t \delta_{eff}$ of equation (34) for monatomic gases.

To illustrate the significance of radiation energy losses note that at 2.7×10^{22} argon atoms per m^3 (corresponding to 370 microns tank

pressure and a free jet static temperature of 100 ^{o}K) and an electron temperature of 10,500 ^{o}K, the total line radiation intensity from an argon plasma is approximately 3.0 watts/cm^{3} (ref. 29) if the population of the radiating states is in equilibrium with the electron temperature. At an illumination power of 1 watt, this radiation loss is about 1000 times larger than the ohmic heating given by equation (41) for argon. However, to obtain a truer measure of the significance of radiation energy losses, we must compare the term $(3/2)\,k\,n_e\,\nu_t\,\delta_{eff}$, with units of W/^{o}K - m^{3}, to the term $\partial\dot{R}/\partial T_e$ in equation (34). To make this comparison we assume that the line radiation intensity from argon changes with temperature at this density at the same rate as the line radiation from oxygen or nitrogen atoms and that $T_e = T^*$. Then use can be made of the data of Allen (ref. 16) to compare these two terms. At T_e = 4900 ^{o}K, $n_a = 2.7 \times 10^{22}$ argon atoms per m^{3} and $Q_{eA} \approx 2 \times 10^{-20}$ m^{2}, we obtain $\nu_t = 2 \times 10^{8}$ sec^{-1}. Then for $n_e = 7 \times 10^{16}$ and $\delta_A = 2.7 \times 10^{-5}$ we obtain $(3/2)\,k\,n_e\,\nu_t\,\delta_{eff} = 7.8 \times 10^{-3}$ W/^{o}K - m^{3} or 7.8×10^{-9} W/^{o}K - cm^{3}. From the data of Allen we obtain at $T^* \approx 4900$ ^{o}K and at the same number density of argon atoms, $\Delta\dot{R}/\Delta T^* = \dot{R}_{4900} - \dot{R}_{3900}/1000 \approx \dot{R}_{4900}/1000 \approx 40 \times 10^{-9}$ W/^{o}K - cm^{3} (ref. 16). Therefore, the term $\partial\dot{R}/\partial T_e$ appears to be much larger than $(3/2)\,k\,n_e\,\nu_t\,\delta_{eff}$ at 4900 ^{o}K and cannot be neglected. Naturally, the excitation temperatures T^* (which are usually equal to $T_{e,E=0}$ under the conditions of the experiment) are not quite as high in the results of table III. However, the departure of the argon gas in the jet from local thermodynamic equilibrium is so strong, as evidenced by the magnitude of $T_{e,E=0}$, that only actual measurements of the radiation losses from the gas can settle the question of the influence of $\partial\dot{R}/\partial T_e$ and instill confidence in the precision of the results of the determination of δ_A.

Careful estimates of the rate of ionization and recombination within the waveguide under the conditions of the experiment seem to exclude the possibility of significant errors in the measurements due to these reactions. However, at this time we can only speculate on the influence of the concentration and rates of excitation and de-excitation of metastable

argon atoms on the magnitude of the term $\sum_i s_i \epsilon_i$ and its effect on the measurements.

An alternative approach would be to include the effect of radiation losses and reaction processes in the quantity δ_{eff} determined by these experiments as a function of T_e and T_g by summing the terms $(3/2)\, k n_e \nu_t \delta_{eff}$ and $\partial \Phi / \partial T_e$ and expressing them in terms of an equivalent δ_{eff}, δ_{eq}, defined by

$$\delta_{eq} \equiv \delta_{eff} + \left(\frac{2}{3 k n_e \nu_t}\right) \frac{\partial \Phi}{\partial T_e} \tag{44}$$

This is a highly artificial approach since it masks many important effects. For example one cannot assess from it the influence of geometry and the relative importance of radiation losses and reaction processes. Therefore results obtained in this way are of doubtful predictive value.

Experiments with Nitrogen

When the experiment was carried out with nitrogen under such conditions that, at the probe location, the nitrogen was molecular and the electron temperature with zero applied electric field, $T_{e, E=0}$, was always equal to an excitation temperature T^* that could be closely identified to the vibrational temperature, T_{vib}, of the nitrogen molecules (see table II), it was found that the temperature $T_{e, E=0} = T^* = T_{vib}$ was always much higher than the static temperature computed by an isentropic expansion from the conditions of the plenum chamber (stagnation pressure $P_o \approx 0.5$ to 1.0 atm and stagnation temperature $T_o = 1500$ - $3500\ ^{o}K$) to the vacuum tank pressure (200 to 1000 microns). In addition, when the vibrational relaxation time was longer than the time of flight of the molecules from the plenum chamber to the probe, the vibrational excitation temperature T_{vib} for the nitrogen molecules at the probe was approximately equal to or higher than the stagnation temperature T_o in the plenum chamber (but always less than the excitation temperature in

the arc). Thus in the absence of an electric field, the electron temperature is in equilibrium with the vibrational excitation temperature of the molecular nitrogen T_{vib} and we can write $T_{e,E=0} = T_{vib} \gtrsim T_o$. Therefore, we can write $T_n = T_g = T_{e,E=0} = T_{vib}$ in equations (5) and (17) and the appropriate temperature that characterizes the energy state of the gas is $T_{vib} = T_{e,E=0}$ as far as the energy-loss factor is concerned. The coupling and equilibration of the free-electron and N_2 vibrational temperatures under essentially similar conditions (but in the presence of an excess of argon) has also been established by Hurle and Russo (ref. 30).

Note that $\delta_{N_2,el} = 3.9 \times 10^{-5}$ while Crompton and Sutton (ref. 18) give, for δ_{N_2}, at $T_g = 288\ ^oK$, $\delta_{N_2} = 3.33 \times 10^{-4}$ at $T_e = 893\ ^oK$, $\delta_{N_2} = 2.90 \times 10^{-4}$ at $T_e = 3140\ ^oK$, $\delta_{N_2} = 3.28 \times 10^{-4}$ at $T_e = 5260\ ^oK$ and $\delta_{N_2} = 8.20 \times 10^{-4}$ at $T_e = 9060\ ^oK$. As a consequence of the fact that at $T_g = 288\ ^oK$ the energy-loss factor for N_2 is nearly constant over the temperature range $893\ ^oK < T_e < 5260\ ^oK$ we can use equation (20) in a simplified form given by (see equation (43))

$$\delta_{eff} = 0.287 \frac{P}{T_e - T_{e,E=0}} \tag{45}$$

where the constant 0.287, corresponding to $Z = 387\ \Omega$, is the result of a compromise that partly compensates for the high values of δ_A determined when an impedance of $420\ \Omega$ is used. The lower value of Z is also used in all determinations of δ_{eff} for N_2-O_2 mixtures reported here.

Typical results of the variation of the measured electron temperature with rf power in nitrogen at 0.9 mm Hg are shown in table IV. For these runs $T_o = 3230\ ^oK$, as obtained from an average enthalpy derived from an arcjet energy balance. Typical values of δ_{N_2} as a function of gas temperature are shown in table V. The results of five or more runs are averaged for each T_g, with typical spreads as in table IV. Equation (45) was used to obtain all data in tables IV and V, although the last four entries of table V are slightly beyond the range where equation (45) was intended to be used.

As far as could be determined the species concentrations at the probe were not at equilibrium with $T_{e,E=0} = T_{vib}$ but at a much lower temperature (see also reference 12). Therefore, the gas at the probe was almost pure N_2 and the values of δ_{eff} tabulated in tables IV and V should correspond to δ_{N_2}. However, although "resonances" in δ_{N_2} with T_g cannot be excluded, it is felt that the variations in the tabulated results are due to impurities in the gas (welder's grade bottled gases, water pumped, with large variations in impurities) and/or leaks in the apparatus. It was observed, for example, that the values of δ_{eff} obtained in these experiments changed (a) quite frequently, by small amounts, when the exhausted gas cylinders were replaced by new ones and (b) always when oxygen was deliberately leaked into the gas feed line in small quantities (approximately 0.5%). Air leaks were found in the apparatus sometime after the two series of runs corresponding to T_g = 1750 and 3480 ^{o}K of table V were carried out. The observed increase of $\delta_{eff} = \delta_{N_2}$ at T_g = 5950 ^{o}K may be due to increased elastic losses due to the rather high electron temperature. The observed decrease of δ_{eff} at T_g = 6100 ^{o}K may be due to an increase of the atom concentration. Whether indeed an increase of 150 ^{o}K in T_g can change the atom concentration sufficiently to cause the observed shift in the value of δ_{eff} is still a matter of conjecture. On the other hand, the temperatures in these last few entries of table V are beyond the range where equation (45) was intended to be used and therefore this behavior is not surprising.

Typically in these experiments with nitrogen we would expect the quantity $(3/2)\, k n_e \nu_t \delta_{eff}$ to be larger by one or two orders of magnitude than the value it has in the argon experiments. Thus at T_e = 3600 ^{o}K, for $n_a = 10^{22}$ N_2 molecules/m^3, $n_e = 7 \times 10^{16}$ electrons/m^3 and $Q_{eN_2} = 9 \times 10^{-20}$ m^2, we obtain $(3/2)\, k n_e \nu_t \delta_{eff} = 2.4 \times 10^{-1}$ watts/^{o}K - m^3. Since the main contribution to the energy radiated from a nitrogen plasma at these temperatures and pressures comes from $N_2(1+)$ and atomic line radiation (i.e., from electronically excited states) and since the radiative lifetimes for spontaneous emission for these transitions is short (of the order of 10 μ sec or less) and the population of these excited states is at

equilibrium at a temperature much lower than $T_{e, E=0}$, the radiation term $\partial \dot{R}/\partial T_e$ and the term $\partial (\sum_i s_i \epsilon_i)/\partial T_e$ can be neglected for all illumination power increments more than 0.2 watts.

As a consequence of the discussion elsewhere in this report, the energy-loss factor for hot nitrogen at equilibrium at a temperature T_g is expected to be the same as the energy-loss factor at $T_g = T_{e, E=0}$ tabulated in table V.

Experiments with Nitrogen-Oxygen Mixtures

Typical values of δ_{eff} for N_2-O_2 mixtures as a function of the mole fraction of oxygen, $M_f = [O_2]/([O_2] + [N_2])$, where the quantities in brackets denote particle concentrations in number/m^3, are shown in table VI and figure 3. These results were obtained by setting the arcjet power controls so as to attain a stagnation enthalpy of approximately 3×10^6 to 4×10^6 joules/kg with pure N_2 (corresponding to T_o = 2500 - 3200 °K) and then introducing an increasing amount of O_2 in the secondary N_2 flow to the plenum chamber while the total flow rate was kept approximately constant by simultaneously decreasing the flow rate of secondary N_2. The primary flow (i.e., the flow through the arc chamber) was pure N_2 and was kept constant. Mixing of the two streams in the plenum chamber was assured by a long-enough residence time (of the order of 1 m sec) and the evidence obtained by color photography, radial surveys of the ion and electron currents and the electron temperature in the plasmajet seemed to confirm that mixing of the two gas streams (i.e., the hot primary N_2 and the cold secondary mixture of N_2 and O_2) was perfect (see Appendix C).

What is immediately apparent from the results of table VI and figure 3 is that even a small amount (~4%) of O_2 helps to de-excite the vibrationally hot pure N_2 from an average $T_g = T_{vib} = T_{e, E=0}$ = 3450 °K (for the four pure nitrogen runs) to an average T_g of approximately 1950 °K (for the four mixture runs at $M_f \approx 0.04$). It appears that the degree of de-excitation increases and the effective gas temperature

T_g decreases as the oxygen content increases but not by as large an amount. For example, from the four runs at an average $M_f \approx 0.32$, we obtain $T_g \approx 1550\ ^{\circ}K$. Therefore, the mixture data presented in table VI and figure 3 correspond to an average gas temperature T_g of $1700\ ^{\circ}K$. For this reason, the pure N_2 value of δ_{N_2} at $T_g = 1700\ ^{\circ}K$ should be taken as the value corresponding to the mixture data of table VI and figure 3. Reference 1 gives $\delta_{N_2} = 2.9 \times 10^{-4}$ at $1700\ ^{\circ}K$. We note that these values of δ_{eff} appear reasonable. For example, for air ($M_f \approx 0.21$) at room temperature, Ginzburg and Gurevich (ref. 7) obtain $\delta_{air} = 1.2 \times 10^{-3}$ at $T_e = 2000\ ^{\circ}K$ and $\delta_{air} = 1.6 \times 10^{-3}$ at $T_e = 3000\ ^{\circ}K$, while Hake and Phelps (ref. 31) report 1.7×10^{-3} for the energy-loss factor at a "characteristic energy" of 0.2 ev. These values compare well with $\delta_{air} = 3 \times 10^{-3}$ obtained from figure 3 for air at a temperature in the vicinity of $1700\ ^{\circ}K$.

An accurate estimate of the term $\partial\Phi/\partial T_e$ in N_2-O_2 mixtures cannot be made since the radiated power is a strong function of the concentration of nitric oxide present in the mixture and there are no reliable estimates of [NO]. On the other hand, the magnitude of the term $(3/2)\, k n_e \nu_t \delta_{eff}$ is even larger in these mixtures than it is in pure nitrogen and it is possible that it remains larger than $\partial\Phi/\partial T_e$ for all mixture ratios.

DISCUSSION OF RESULTS AND CONCLUSIONS

There is not much else that needs to be said concerning the results for argon and nitrogen presented in tables II and V. If anything, these results are surprisingly close to the expected values for argon and appear reasonable for nitrogen in the sense that they are within ~10% of the reported room temperature values at low gas temperature ($T_g < 2000\ ^{\circ}K$) where appreciable vibrational excitation has not yet taken place and they show an increase of δ_{eff} for hotter nitrogen as compared to nitrogen at $288\ ^{\circ}K$, a trend expected from theoretical considerations [see, for example, equation (42)].

Although the reproducibility and accuracy of the results for N_2-O_2 mixtures plotted in figure 3 could be considered satisfactory, there are two disturbing factors: When we use the consistent terminology of Demetriades and Argyropoulos (ref. 3) for the definition of collision frequencies $\tau_{e,\kappa}$ and cross-sections $Q_{e\kappa}$ for collisions between electrons and heavy particles, the mixture rule of reference 1 (assuming only N_2 and O_2 present), and the values of $\delta_{N_2} = 3 \times 10^{-4}$, $R_Q = Q_{eN_2}/Q_{eO_2} = 2.5$ and 2.0, we derive for the energy-loss factor δ_{O_2} of pure oxygen in the vicinity of 1700 °K the values listed in the last two columns of table VI. These values of δ_{O_2} (2×10^{-2} to 3×10^{-2}) are a little high. Thus if $\delta_{O_2} = 6.7 \times 10^{-3}$ when $T_e \approx 2000$ °K and the gas is at room temperature (ref. 7), and if the pattern set in the nitrogen experiments (ref. 1) is followed by O_2, one would <u>not</u> have expected δ_{O_2} to be much higher at 1700 °K than at room temperature. A clue as to the possible source of this anomaly is provided in table VII, where we see that the values derived for δ_{O_2} by the mixture rule are dependent on the oxygen content. The source of this dependence appears to be the effect on the computation of δ_{O_2} of the presence of nitric oxide, NO, and atomic oxygen, O, in the mixture. In other words the assumption that N_2 or O_2 are the only species present breaks down. For example, we can show that at the lower oxygen concentrations, the assumption of a small concentration of NO is sufficient to decrease the computed value of δ_{O_2} for pure O_2 by a factor of 2 or 3, because of the largeness of δ_{NO} (ref. 32), even though the contribution of NO to the observed δ_{eff} for the mixture is small. At the higher oxygen content, the assumption of a small concentration of atomic oxygen is sufficient to increase the computed value of δ_{O_2} by a smaller but still significant amount. It is quite likely that both species are present in small but significant amounts as far as the computation of δ_{O_2} by the mixture rule is concerned. Electron attachment to O_2 may also make a significant contribution to the observed values of δ_{eff}. These are typical of the difficulties caused by the proliferation of variables due to chemical changes. Nevertheless, good accuracy can be expected in the <u>observed</u> δ_{eff} data for <u>mixtures</u> since the concentrations of both NO and O are probably small.

Careful determinations of the composition in the plasmajet or operation with other gases (such as argon-nitrogen and argon-oxygen mixtures instead of N_2-O_2) are expected to remove this source of uncertainty in the data.

The other disturbing factor is the rather unusual spread in the data at higher oxygen concentrations, especially when the intrinsic simplicity and accuracy of this method for the determination of δ_{eff} is taken into consideration. Several sources appear to be contributing to this spread. Some of these are: (a) oxidation and surface contamination or aging of the tungsten probes; (b) noise in the arcjet; (c) the increase in the number of variables especially in such mixtures as N_2-O_2 that makes it difficult to maintain one quantity constant while varying others*; and (d) the human factor in data reduction (especially of the Langmuir probe data where a certain minimum level of practice is required). All these sources of uncertainty, including the influence of $\partial\Phi/\partial\bar{T}_e$ and especially the effect of radiation losses, need to be systematically attacked since it is felt that even small variations in the value of δ_{eff} with gas temperature can have a very significant effect on the performance and stability of $J \times B$ and other devices (refs. 2, 33).

On the whole, the mixture energy-loss factors determined directly by this initial experiment and presented here are considered accurate within a factor of $(2)^{\pm 1/2}$ or better at low O_2 concentrations. At higher O_2 concentrations ($M_f > 0.3$) the additional complication of possibly significant departures from a Maxwellian electron energy distribution may have contributed to the spread of the data. Under such conditions the lower rf power runs should be more reliable (since they perturb the initial Maxwellian least).

---

* For example, in these mixtures δ_{eff} is a function not only of T_e and T_g but also of $[O_2]/[N_2]$, the stagnation enthalpy and pressure in the arc chamber and the pressure in the vacuum tank – as a result even the job of presenting the data becomes very complicated.

The values for the energy-loss factor for heated pure oxygen derived by processing the mixture data are not as reliable but it would be surprising if the exact values do not fall within the spread of data, $\sim(2)^{\pm 1}$, presented here.

It is believed that the main sources of error associated with the equipment are: (a) drift of the Langmuir probe characteristics due to long-term fluctuations in the arcjet current-voltage characteristics caused by the wandering of the arc attachment spots on the anode and cathode and (b) noise due to intermittent arc operation or rotation as well as 60-Hz ground loops. The extent to which these sources of error affect the reproducibility and accuracy of the measurements is still a matter of conjecture.

The fact remains that the experimental results follow very closely the expected values of the energy-loss factor for three different gases over two and one-half orders of magnitude. Moreover, this method for determining the electron energy-loss factor, and therefore also the collision cross-sections for energy transfer between slow electrons and heavy particles, possesses two very significant and favorable features: (1) all important measurements are dc and (2) since the energy-loss factor has been uncoupled from (a) the collision frequency, or (b) the drift velocity and the diffusion coefficient, it can be determined independently of collision cross-sections for momentum transfer and particle densities.

ACKNOWLEDGMENTS

I want to thank C. H. Deichler, J. C. Sutton and A. D. Varvatsis of our laboratory for superior performance in the design and fabrication of all the specialized apparatus used in these experiments and Drs. G. S. Argyropoulos and K. Lackner of our staff for many helpful suggestions and discussions. I also want to thank Miss Susan Hagen for reduction of much of the data presented in this and previous publications, and M. Caloyannides for performing and reducing some of the N_2-O_2 mixture experiments. Thanks are also due to Prof. S. L. Petrie for the design of the electron beam apparatus and for many helpful discussions. Finally I want to thank Mr. Howard Stine of NASA/Ames for his patience and support.

APPENDIX A

DIMENSIONS OF WAVEGUIDE AND ESTIMATE OF WAVE IMPEDANCE

In choosing the dimensions of the waveguide several factors should be taken into account.* These are:

(1) The operating dominant mode of electromagnetic wave propagation in the waveguide, TE_{10}, will excite higher modes because of the presence of obstacles (quartz tube containing the plasma, probe, etc.) inside the waveguide. In the steady state not all of the higher modes carry real power because, depending on the dimensions of the guide and the operating frequency, some of them can be made evanescent. The TE_{10} scattered mode will enter in the series expansion for the scattered field (in terms of the waveguide modes) with the largest coefficient and can be termed the reflected wave as though only the TE_{10} existed. Then an estimate of the coefficient of the reflected wave can give information about the coefficients of the higher modes that can be excited.

(2) The holes on the sidewalls through which the plasmajet flows should not appreciably obstruct the flow of currents which sustain the propagating mode.

(3) The holes in the sidewalls should be large enough so that they

---

* For a more detailed review of the subject of electromagnetic wave propagation, waveguides and related measurements see (1) Ginzton, Edward L.: Microwave Measurements, McGraw-Hill Book Company, Inc., New York (1957); (2) King, Donald D.: Measurements at Centimeter Wavelength, D. Van Nostrand Company, Inc., New York (1952); (3) Reich, Herbert J.; Ordung, Philip F.; Krauss, Herbert L.; and Skalnik, John G.: Microwave Theory and Techniques, D. Van Nostrand Company, Inc., New York (1953); (4) Wind, Moe; and Rapaport, Harold (eds.): Handbook of Microwave Measurements, Microwave Research Institute, Polytechnic Institute of Brooklyn (1955); (5) Sommerfeld, Arnold: Electrodynamics, Academic Press, Inc., New York (1964); (6) Goubau, George: Electromagnetic Waveguides and Cavities, Pergamon Press, New York (1961).

do not appreciably obstruct the flow of the free jet of plasma.

(4) The characteristic time of flow of the plasma across the waveguide should be much greater than the relaxation time of the electron temperature to ensure an almost instantaneous steady-state response of the electron temperature to the local field so that the formula giving $T_e - T_g$ in terms of the electric field be applicable.

Let us consider the influence of each one of these design constraints in selecting the dimensions of the waveguide.

The magnitude of the wave vector of the TE_{nm} mode in a rectangular waveguide is given by

$$k = \left[k_o^2 - \left(\frac{n\pi}{a}\right)^2 - \left(\frac{m\pi}{b}\right)^2 \right]^{1/2} \qquad \text{(A-1)}$$

where a, b are the width and height of the waveguide respectively (see Fig. 1, Appendix A), n, m are integers not both zero, $k_o = \omega/c = 51.34\ m^{-1}$ and $\omega = 1.54 \times 10^{10}$ rad sec at $f = 2.45$ GHz.

A propagating mode should satisfy the inequality

$$k_o^2 > (n\pi/a)^2 + (m\pi/b)^2 \qquad \text{(A-2)}$$

therefore, we may choose a, b such that this inequality is <u>not</u> satisfied for a given n, m and consequently any given TE_{nm} mode will be evanescent, carrying no real power. For example, if we want only the TE_{10} mode to propagate down the waveguide we should choose $2b < \lambda_o = 0.122\ m < 2a$. The condition $2a > \lambda_o$ ensures that TE_{10} propagates but does not exclude other modes from propagating. However, because of factors (2), (3) and (4) we <u>cannot</u> choose a, b such that <u>only</u> the dominant mode TE_{10} should propagate. Thus factors (2) and (3) require that $b \geq 4" = 0.1016\ m$ and factor (4) that $a \geq 6" = 0.1524\ m$. If we, therefore, choose $a = 6" = 0.1524$ m, and $b = 4" = 0.1016$ m, we can easily show that the following modes can propagate and consequently carry real power:

$$TE_{10},\ TE_{20},\ TE_{01},\ TE_{11}$$

(We do not have to worry about TM modes because we know that even if they get excited by the TE_{10} mode they will have a negligible coefficient simply because the exciting mode is a TE_{10} mode and not a TM_{11} mode.)

We now make an estimate of the coefficient of the reflected wave (= scattered TE_{10}).

The tube containing the plasma is made of quartz with an index of refraction approximately 2 in the microwave frequency range of the experiment. The index of refraction of the plasma in a good approximation is given by $\eta = [1 - (\omega_p^2/\omega^2)]^{1/2}$.

For a maximum ω_p^2 equal to $0.25\ \omega^2$ we obtain $\eta \approx 0.867$. The plasma column will have a diameter of about 2.5" or 0.0625 m therefore the ratio of the power reflected to the incident power for a plasma slab of thickness $d \approx 2"$ or 0.05 m is

$$\rho = \frac{2s\,[1 - \cos(2kd\eta)]}{1 + s^2 - 2s\cos(2kd\eta)} \qquad \text{(A-3)}$$

where

$$s = \left(\frac{\eta - 1}{\eta + 1}\right)^2, \quad k = [k_o^2 - (\pi/a)^2]^{1/2} \approx 46\ m^{-1}$$

Therefore the <u>maximum</u> power reflected from the plasma ρ_p is 1.7 percent of the incident power. For a quartz thickness $d \approx 0.001$ in the reflectivity of the quartz (slab) ρ_Q will be ≈ 0.58 percent. The resulting ρ is of the order of the sum $\rho_p + \rho_Q$ because the index of refraction of the plasma is close to unity.

The above rough estimate of the coefficient of the reflected field and power assures that the coefficient of the higher modes will be small compared to the TE_{10} mode so that the power carried by the non-evanescent scattered modes will be negligible compared to the power carried by the incident dominant mode TE_{10}. This last conclusion is further

supported by the fact that the wave impedance of a mode increases with the order of the mode (see below).

Wave Impedance

When $\partial\delta_{eff}/\partial T_e \approx 0$, as we have already explained in the text, following equation (19), the electron energy-loss factor δ_{eff} is given by

$$\delta_{eff} = \frac{e^2}{3km_e\omega^2}\left(\frac{4Z}{A_r}\right)\cdot\left(\frac{dT_e}{dP}\right)^{-1} \tag{A-4}$$

Where Z = impedance of the gap in the waveguide, P = power and A_r = the cross-sectional area of the waveguide. Now, in general, a propagating TE_{nm} mode, when n, $m \neq 0$, carries a power given by

$$P_{nm} = \frac{ab}{4}\,\frac{\{|E_{ox}|^2 + |E_{oy}|^2\}}{2Z_{h,nm}} \tag{A-5}$$

or, when $m = 0$ and $n \neq 0$,

$$P_{n0} = \frac{ab}{4}\,\frac{|E_{oy}|^2}{Z_{h,n0}} \tag{A-6}$$

with

$$Z_{h,nm} = \frac{kZ}{\left[k^2 - \left(\frac{n\pi}{a}\right)^2 - \left(\frac{m\pi}{b}\right)^2\right]^{1/2}} \tag{A-7}$$

where

$$Z = \left(\frac{\mu}{\epsilon}\right)^{1/2} \quad \text{and} \quad k = \frac{\omega}{v_{ph}} = \frac{\omega\eta}{c} = k_o\eta$$

where μ, ϵ, η, are the permeability, permitivity and index of

refraction $[\eta = (\mu\epsilon/\mu_o\epsilon_o)^{1/2}]$ respectively of the medium by which the guide is filled.

For vacuum and the dominant mode we obtain $Z_{h,10} = 1.09\, Z_o$ where $Z_o = (\mu_o/\epsilon_o)^{1/2} = 377\,\Omega$. For the plasma in question with max ω_p (worst case) we obtain $Z_{h,10} = 1.3\, Z_o$. Therefore the actual $Z_{h,10}$ should be such that

$$1.09\, Z_o < Z_{h,10} < 1.3\, Z_o \qquad \text{(A-8)}$$

and of course it will be closer to $1.09\, Z_o$ than to $1.3\, Z_o$. (We do not have to consider the effect of the quartz tube since $2\pi k = \lambda_g >> d$ where d is the quartz thickness).

Now from equation (A-6) the amplitude of the electric field will be given by

$$E_o^2 = \frac{4P}{ab} \cdot Z_{h,10} \qquad \text{(A-9)}$$

and Z in equation (A-4) is properly given by $Z_{h,10}$ while the area in equation (A-4) is given by $A = ab/4$. The average electric field E^2 will be given by $2E^2 \equiv 2\langle E^2\rangle = E_o^2$. The origin of the factor 4 in equation (A-9) can be interpreted to be the result of two averagings over time and space. As P in equation (A-4) we may use the power transmitted through the guide. This power will be measured by the apparatus we have designed and will be given to good approximation, at the center of the waveguide where T_e is measured, as the power input to the waveguide plus the power output divided by two (this accounts for connector and waveguide losses). Thus P usually amounts to 80% of the input or nominal power.

The power losses in the plasma have been shown to be negligible under the conditions of the experiment.

Numerical values of the grouping $[e^2/(3km_e\omega^2)]\,(4Z/A_r)$ that appears in equations (19), (20) and (A-4) as a function of the impedance Z at f = 2.45 GHz are given in the following tabulation:

$$Z = Z_o = 377\,\Omega, \qquad \delta_{eff} = 0.280\,(\Delta P/\Delta T_e)$$

$$Z = 387\,\Omega, \qquad \delta_{eff} = 0.287\,(\Delta P/\Delta T_e)$$

$$Z = 400\,\Omega, \qquad \delta_{eff} = 0.297\,(\Delta P/\Delta T_e)$$

$$Z = 1.09\,Z_o = 411\,\Omega, \qquad \delta_{eff} = 0.305\,(\Delta P/\Delta T_e)$$

$$Z = 1.3\,Z_o = 490\,\Omega, \qquad \delta_{eff} = 0.363\,(\Delta P/\Delta T_e)$$

Numerical values of some other groupings of interest are given in the following tabulation for $f = 2.45$ GHz ($\omega = 1.5393 \times 10^{10}$ rad/sec) and mks units:

$$\frac{e^2}{2m_e\omega^2} = 5.947 \times 10^{-29}, \qquad \frac{2}{3k} = 0.4829 \times 10^{23}$$

$$\frac{e^2}{3km_e\omega^2} = 0.2871 \times 10^{-5}, \qquad \frac{3k\delta_{A,el}}{2} = 5.645 \times 10^{-28}$$

while for $Z = 387$ ohms and $A = 0.1016\ \text{m} \times 0.1524\ \text{m} = 1.548 \times 10^{-2}\ \text{m}^2$ we obtain

$$E_o^2 = (4Z/A_r)\,P = 1.0 \times 10^5\,P$$

where P is in watts.

APPENDIX B

SENSITIVITY OF THE MEASUREMENTS

At 2.45 GHz ($\omega = 1.54 \times 10^{10}$ rads/sec) the quantity $2e^2/(3km_e\omega^2)$ is equal to $4 \times 10^{15}/(3 \times 2.4 \times 10^{20}) = 5.74 \times 10^{-6}$, mks units. Therefore if $T_e = f(E_o)$ is measured we have* from equation (20) in mks units

$$\delta = 5.74 \times 10^{-6} E_o \left(\frac{dT_e}{dE_o}\right)^{-1}$$

Let us assume that at a given gas temperature T_g a plot of T_e is obtained as a function of E_o and that for our purposes $E = 0.707\ E_o$. Then we can read the corresponding slope dT_e/dE_o and E_o at any T_e and obtain δ. We have said that the quantity δ should not vary more than a few percent within narrow ranges of T_e. Therefore at a given T_g the quantity $E_o \cdot dE_o/dT_e$ or $E_o(dT_e/dE_o)^{-1}$ should be constant at approximately $2 \times 10^5\ \delta$ in mks units. For example, if, at $T_e = 4000\ ^oK$ and a given T_g, the electric field is $E_o = 10$ volts/cm $= 10^3$ volts/m and $dE_o/dT_e = 0.5$ volts/(m - ^oK) or $dT_e/dE_o = 2\ ^oK$ - m/volt, we obtain $\delta = 2.8 \times 10^{-3}$. Then also at $T_e = 3000\ ^oK$ (and the same T_g) and at $E_o = 5$ volts/cm, we must read approximately $dE_o/dT_e \approx 1$ or $dT_e/dE_o \approx 1$ in mks units. The slope of T_e vs. E_o will be proportional to E_o. If T_e can be measured within $\pm 100\ ^oK$, a range of at least $1000\ ^oK$ must be available for T_e variation to ensure good accuracy and the required change of E_o over the interval must range, conservatively, between 0.1 volt/m per ^oK and 1 volt/m per ^oK. Since it will be possible to vary E_o by <u>hundreds</u> of volts/m (1 volt/cm = 100 volts/m) we should be able to obtain changes of <u>one thousand or more</u> ^oK in electron temperature and therefore it seems possible to obtain values of δ with good precision. Operation at higher T_e and E_o will enhance this precision if the error in measuring T_e remains the same.

*In this Appendix, we omit the subscript "eff" from δ, for simplicity.

From equation (17), with $\nu_t^2 >> \omega^2$, we obtain

$$\delta = \frac{e^2 E_o^2}{3 k m_e \omega^2 (T_e - T)}$$

Now let us consider the error, $\Delta\delta$, in δ, resulting from the uncertainties ΔE_o and ΔX ($X = T_e - T_n$) when δ is determined from a single measurement of E_o and X. The error $\Delta\delta$ will be given by the familiar expression

$$\Delta\delta = \left|\frac{\partial\delta}{\partial X}\right| \Delta X + \left|\frac{\partial\delta}{\partial E_o}\right| \Delta E_o$$

now

$$\frac{\partial\delta}{\partial X} = -\frac{e^2 E_o^2}{3 k m_e \omega^2 X^2} \quad \text{and} \quad \frac{\partial\delta}{\partial E_o} = \frac{2 e^2 E_o}{3 k m_e \omega^2 X}$$

hence

$$\Delta\delta = \frac{e^2 E_o^2}{3 k m_e \omega^2 X^2} \Delta X + \frac{2 e^2 E_o}{3 k m_e \omega^2 X} \Delta E_o$$

$$= \delta \left(\frac{\Delta X}{X} + \frac{2 \Delta E_o}{E_o}\right)$$

This gives the relative error in δ which is

$$\frac{\Delta\delta}{\delta} = \frac{\Delta X}{X} + \frac{2 \Delta E_o}{E_o}$$

Since $\Delta X = |\Delta T_e| + |\Delta T_n|$, if we can assume that $\Delta T_e = 100\ ^oK$, $\Delta T = 50\ ^oK$ and $X \equiv T_e - T_n = 10^3\ ^oK$ while $\Delta E_o = 100$ volts/m and $E_o = 10^3$ volts/m, we obtain, for the relative error in δ

$$100 \times \frac{\Delta\delta}{\delta} = 100 \times \left(\frac{100 + 50}{1000} + \frac{2 \times 100}{1000}\right) = 35\%$$

It is important to realize that this error is the maximum error that can occur at these values of E_o and X and when only these two measurements are made. Even for such single measurements there is a probability that the errors in T_e, T_n and E_o will partially cancel. The situation is even more favorable for the experiments described in the text because many measurements of differing E_o and T_e have been made in determining the value of δ corresponding to a given T_n (i.e., in determining the slope dT_e/dE_o). When δ is obtained from such multiple measurements then the error is greatly reduced by averaging effects.

An evaluation of the results presented in the literature on measurements of $\delta = f(T_e)$ appears to indicate that other methods for evaluating δ (by swarm techniques) are less accurate than the method described here.

APPENDIX C

EXPERIMENTAL PROBE CHARACTERISTICS; SURVEYS OF ELECTRON AND ION CURRENTS AND ELECTRON TEMPERATURES; TYPICAL ROTATIONAL AND VIBRATIONAL SPECTRA

Figures 1C and 2C of this Appendix are traces of the probe current-voltage characteristics obtained for nitrogen on the x-y recorder with and without rf illumination power. In figure 1C the characteristics were traced twice and in figure 2C five separate times for each recorder sensitivity setting. This procedure of tracing the probe characteristics more than once on each recording sheet was established and carried out routinely in all runs in order to provide a visual indication of drift or excessive noise.

Figures 3C and 4C of this Appendix represent a radial and axial survey, respectively, of the electron and ion currents in the plasmajet with the Pt-Ir gas-cooled probe. The radial survey, figure 3C, was carried out by traversing the probe on the z-axis, i.e., perpendicular to the plasmajet axis (x-axis), at a distance of approximately 0.35 m downstream from the arcjet nozzle at a fixed operating condition (i.e., constant mass flow rate and power) corresponding to a stagnation temperature of approximately 2500 ^{o}K. The uncertainty in locating the jet axis is less than ± 0.05". Note that the probe was traversed from left to right and then returned from right to left (i.e., it started 2" to the left of the plasmajet axis as we look down the axis of the tank from outside the tank door and continued traversing past the jet axis or centerline to 2" to the right of the plasmajet axis and then returned back to its original position 2" to the left of the plasmajet). Note the perfect azimuthal symmetry of the electron and ion current distributions. Since this symmetry of the jet was obtained when 50% of the flow rate was injected into the plenum chamber downstream of the arc, it is concluded that the primary and secondary gases mix perfectly in the plenum chamber.

In the axial survey, figure 4C, the sharp peaks in electron current correspond to passage of the probe through the apex of the shock diamonds

in the supersonic plasmajet. Note that the peaks in ion current lag the peaks in electron current. This axial survey was obtained by placing the probe at the exit plane of the nozzle and withdrawing it along the jet axis. This procedure was followed for both the electron and ion current traces. The probe location was checked repeatedly during the production of both traces and there was perfect spatial coincidence, i.e., there can be no question of the ion-current trace being displaced with respect to the electron current trace. The coincidence of the bottom of the valleys in both traces confirms the spatial coincidence of the two traces. No drifts were observed in the arcjet characteristics during the recording of these traces. A total of eight clearly-detectable probe-current peaks were obtained when the probe was traversed up to a distance of 35" from the nozzle exit plane, corresponding to an equal number of shock diamonds.

Clearly, the results of the axial survey indicate that the probe should not be located near or at the apex of a shock diamond since large concentration and/or electron temperature gradients occur there and the conditions leading to equation (16) may be violated.

Figures 5C and 6C are the results of a radial and axial electron temperature distribution survey, respectively.

Comparing the results of figures 3C and 5C we see that although the electron temperature remains very nearly constant across the jet, (from +1.0" to -1.00") the ion current goes from essentially zero to its maximum of 0.375 mv in the same interval ($2.5 \times 0.81 \approx 2.0$"). At the same time, the electron current decreases less rapidly than the ion current. Thus the ion current reaches 10% of its peak centerline value within 0.8" from the centerline or jet axis whereas the electron current reaches 10% of its peak value at approximately 1.12" from the centerline. The implication of these observations is that a low-n_e high-T_e sheath surrounds the jet of plasma.

Another interesting observation concerns the increased noise level of the electron current signal as the probe traverses the jet boundary and/or the sheath that becomes apparent in figure 3C. This explains why

some early runs that were made with a probe that was not carefully centered had to be scrapped because of too much noise.

The lack of a clear-cut fine structure or symmetry in the T_e distribution plotted in figure 5C was somewhat of a disappointment which was only partially compensated by the excellent linearity over 2.5 to 3 decades of the probe data for the temperature points plotted in that figure and obtained with the high-sensitivity x-y recorder at 0.1 mv/in. The plasma was pure nitrogen and the probe was the platinum-iridium gas-cooled probe. The uncertainty of each point plotted in figure 5C could not have been more than ±5% and the spread in the data must be due to drift of the arcjet characteristics.

Figure 6C depicts the probe characteristics obtained at different distances from the arcjet nozzle exit plane. The remarkable feature of this survey is the uniformity of the shape of the probe characteristic traces. The uniformity of the slope of these curves testifies to the uniformity of the electron temperature with axial distance (x-axis), at least in the interval from 4 inches (~ 0.10 m) to 19 inches (~ 0.48 m) from the nozzle exit.

Note that if the electron temperature does indeed remain constant or nearly constant through the oblique shock diamonds of figure 4C the peaks in electron current must correspond to increased electron concentration and the peaks in ion current to increased ion concentration. However, this might violate the charge neutrality condition. Therefore, the lag between the electron and ion current peaks must signify that some other significant relaxation effect is taking place – for example, the ion temperature may be changing through the shock diamond apex. This phenomenon has not yet received a satisfactory explanation.

The surveys of figures 2C through 6C were obtained in a free jet of nitrogen plasma corresponding to arc operating conditions similar to those for which $T_{e,\,E=0} \approx 3000\ ^{o}K$ in table V of the text. The waveguide and 2.40-inch O.D. quartz tube surrounding the jet were removed for these surveys.

Figure 7C depicts the probe characteristics obtained in an axial survey within the waveguide cavity (i.e., with the quartz tube and waveguide in place) for approximately the same arcjet operating conditions with rf power on and with rf power off. A clear-cut decrease of the slope of the curves obtained with rf power on as compared to the slope of the curves with rf power off and as the probe location moves toward the cavity center, is apparent. Surveys similar to figure 7C confirm the existence of an electron temperature distribution within the waveguide with rf power on of the form $T_e \propto [E_o \sin(2x/a)]^2$.

Figure 8C shows the effect of rf on the probe electron current. It was obtained by carrying out two traverses with the gas-cooled probe. Each traverse begins at the nozzle exit and continues to about 20" downstream (i.e., past the end of the waveguide). In one traverse the rf power is on and in the other it is off. The important results are that the two traces come together past the end of the waveguide (proving that the electron temperature rise in the waveguide does not produce any persistent effects) and that the shock diamond peaks are enhanced with rf power.

Figures 9C and 10C are typical results of the electron-beam excitation-spectroscopy diagnostic experiments obtained with the apparatus described in the text. Figure 9C shows the rotational band of $N_2^+(0, 0)$ at 3914 Å used to determine rotational temperature and figure 10C shows typical band profiles of the $N_2^+(0, 1)$ progression at 4278, 4236 and 4199 Å, used to determine the vibrational temperature.

Note that the interpretation of these intensity profiles and the probe characteristic traces leads to the conclusion that the vibrational and rotational energy states as well as the free electron temperature seem to have Maxwellian distributions so that T_{vib}, T_{rot} and $T_{e, E=0}$ are well-defined.

REFERENCES

1. Demetriades, S. T.: Determination of Energy-Loss Factors for Slow Electrons in Hot Gases. Phys. Rev., vol. 158, No. 2, June 1967, pp. 215-217.

2. Argyropoulos, G. S.; Demetriades, S. T.; and Kendig, A. P.: Current Distribution in Nonequilibrium J × B Devices. J. Appl. Phys., vol. 38, No. 13, December 1967, pp. 5233-5239.

3. Demetriades, S. T.; and Argyropoulos, G. S.: Ohm's Law in Multicomponent Nonisothermal Plasmas with Temperature and Pressure Gradients. Phys. Fluids, vol. 9, No. 11, November 1966, pp. 2136-2149.

4. Aliyevskiy, M. Y.; and Zhdanov, V. M.: Transport Equations for Nonisothermal Multicomponent Plasma. Zh. Prikl. Mekh. i Tekhn. Fiz., No. 5, (1963) p. 11 [English transl.: J. Appl. Mech. and Tech. Phys., No. 5, September-October 1963, pp. 14-23].

5. Cravath, A. M.: The Rate at Which Ions Lose Energy in Elastic Collisions. Phys. Rev., vol. 36, No. 2, July 1930, pp. 248-250.

6. Zhdanov, V. M.: Transport Phenomena in a Partly Ionized Gases. Prikl. Matem. i Mekh., vol. 26, No. 2, (1962) pp. 280-288 [English transl.: Appl. Math. Mech., vol. 26, No. 2, (1962) pp. 401-413].

7. Ginzburg, V. L.; and Gurevich, A. V.: Nonlinear Phenomena in a Plasma Located in an Alternating Electromagnetic Field. Usp. Fiz. Nauk, vol. 70, No. 2, February 1960, pp. 201-246 [English transl.: Soviet Phys. -Usp., vol. 3, July-August 1960, pp. 115-147].

8. Lutz, M. A.: Radiation and Its Effect on the Nonequilibrium Properties of a Seeded Plasma. AIAA J., vol. 5, No. 8, August 1967, pp. 1416-1423.

9. Cool, T. A.; and Zukoski, E. E.: Recombination, Ionization, and Nonequilibrium Conductivity in Seeded Plasmas. Phys. Fluids, vol. 9, No. 4, April 1966, pp. 780-796.

10. Cool, T. A.: Recombination, Ionization and Nonequilibrium Conductivity in Seeded Plasmas. Ph. D. Thesis, California Institute of Technology (1965).

11. Zukoski, E. E.; Cool, T. A.; and Gibson, E. G.: Experiments Concerning Nonequilibrium Conductivity in a Seeded Plasma. AIAA J., vol. 2, No. 8, August 1964, pp. 1410-1417.

12. Kelly, A. J.; Nerheim, N. M.; and Gardner, J. A.: Electron Density and Temperature Measurements in the Exhaust of an MPD Source. AIAA J., vol. 4, No. 2, February 1966, pp. 291-295.

13. De Leew, J. H.: Electrostatic Plasma Probes in Physico-Chemical Diagnostics of Plasmas. Proceedings of the Fifth Biennial Gas Dynamics Symposium, Northwestern University Press, 1963.

14. (a) Cozens, J. R.; and von Engel, A.: Theory of the Double Probe at High Gas Pressure. International Journal of Electronics, vol. 19, No. 1, July 1965, p. 61; (b) Kagan, Yu. M.; and Perel, V. I.: Probe Methods in Plasma Research. Usp. Fiz. Nauk, vol. 81, No. 3, December 1963, pp. 409-452; (c) Waymouth, J. F.: Perturbation of a Plasma by a Probe. Phys. Fluids, vol. 7, No. 11, November 1964.

15. Kontaratos, A. N. ; and Demetriades, S. T. : Electrical Breakdown of Gases at Elevated Temperatures. Phys. Rev., vol. 137, No. 6A, March 1965, pp. A1685-A1686.

16. Allen, Richard A. : Air Radiation Graphs: Spectrally Integrated Fluxes Including Line Contributions and Self Absorption. AVCO/Everett Research Report 230, September 1965.

17. Morris, J. C. ; Krey, R. V. ; and Garrison, R. L. : Radiation Studies of Arc Heated N_2 , O_2 and Argon Plasmas. AVCO/ RAD, AVSSD-0049-68-RR, March 1968.

18. Crompton, R. W. ; and Sutton, D. J. : Experimental Investigation of the Diffusion of Slow Electrons in Nitrogen and Hydrogen. Proc. Roy. Soc., vol. A215, No. 1123, December 1952, pp. 467-480.

19. Frost, L. S. ; and Phelps, A. V. : Momentum-Transfer Cross Sections for Slow Electrons in He, Ar, Kr, and Xe from Transport Coefficients. Phys. Rev., vol. 136, No. 6A, 14 December 1964, A1538-A1545; also additional data provided by Phelps, A. V. (personal communication).

20. Muntz, E. P. ; and Marsden, D. J. : Electron Excitation Applied to the Experimental Investigation of Rarefied Gas Flows. RAREFIED GAS DYNAMICS, vol. II, J. A. Laurmann, editor, Academic Press, New York, (1963) pp. 495-526.

21. Petrie, S. L. : Flow Field Analyses in a Low Density Arc-Heated Wind Tunnel. Proceedings of the 1965 Heat Transfer and Fluid Mechanics Institute, Andrew F. Charwat et al., editors, Stanford University Press, (1965) pp. 282-300.

22. Petrie, S. L. : Density Measurements with Electron Beams. AIAA J., vol. 4, No. 9, September 1966, pp. 1679-1680.

23. Sebacher, D. I.: An Electron Beam Study of Vibrational and Rotational Relaxing Flows of Nitrogen and Air. Proceedings of the 1966 Heat Transfer and Fluid Mechanics Institute, M. A. Saad and J. A. Miller, editors, Stanford University Press (1966).

24. Muntz, E. P.: Static Temperature Measurements in a Flowing Gas. Phys. Fluids, vol. 5, No. 1, January 1962, pp. 80-90.

25. Mott, N. F.; and Massey, H. S. W.: The Theory of Atomic Collisions. University Press, London (1952).

26. Herzberg, G.: Spectra of Diatomic Molecules. D. van Nostrand and Co., New York (1950).

27. McBride, B. J.; Heimel, S.; Ehlers, J. G.; and Gordon, S.: Thermodynamic Properties to 6000 ^{o}K for 210 Substances Involving the First 18 Elements. NASA SP-3001 (1963).

28. McGregor, W. K.; and Brewer, L. E.: Equivalence of Electron and Excitation Temperatures in an Argon Plasma. Phys. Fluids, vol. 9, No. 4, April 1966, pp. 826-827.

29. Evans, D. L.; and Tankin, R. S.: Measurement of Emission and Absorption of Radiation by an Argon Plasma. Phys. Fluids, vol. 10, No. 6, June 1967, pp. 1137-1144.

30. Hurle, I. R.; and Russo, A. L.: Spectrum-Line Reversal Measurements of Free-Electron and Coupled N_2 Vibrational Temperatures in Expansion Flows. J. Chem. Phys., vol. 43, No. 12, December 1965, pp. 4434-4443.

31. Hake, Jr., R. D.; and Phelps, A. V.: Momentum-Transfer and Inelastic-Collision Cross Sections for Electrons in O_2, CO, and CO_2. Phys. Rev., vol. 158, No. 1, June 1967, pp. 70-84.

32. Phelps, A. V.: Private Communication, gives for the velocity-dependent electron energy-loss factor of nitric oxide, $\delta_{NO} \approx 3\,\delta_{O_2}$ to $5\,\delta_{O_2}$ in the region of $\frac{3}{2}kT_e$ from 0.2 ev to 0.3 ev.

33. Lackner, K.; Argyropoulos, G. S.; and Demetriades, S. T.: Relaxation Effects in J × B Devices. AIAA J., vol. 6, No. 5, May 1968, pp. 949-951.

TABLE I

SUMMARY OF CONSTRAINTS

	Origin	Expression	Implication
1.	Maxwellian distribution of electrons assumed	Equation (20)	$n_e/n_\kappa \gtrsim 10^{-7}$ Sets an upper limit on n_κ for a given n_e. Can be relaxed for small electric field.
2.	Penetration of rf field into plasma	Equation (23)	$n_e \leq \omega^2/324\pi^2$ Sets an upper limit on n_e for a given ω. Can be relaxed if high electron concentration core is only a few electron mean free paths thick.
3.	Frequency of electric field much greater than collision frequency	Equation (24)	$n_a^2 \ll 1.46 \times 10^{-8}\omega^2/Q_{ea}^2 T_e$ Sets an upper limit on density of neutrals.
4.	Langmuir probe size smaller than electron mean free path	Equation (25)	Sets an upper limit on density of neutrals.
5.	Langmuir probe size greater than Debye length	Equation (26)	Sets a lower limit on electron density.

TABLE I

(Concluded)

	Constraints 6 - 11 are associated with the experimental technique chosen to heat the electrons		
6.	Adequate flow time across waveguide	Equation (28)	Sets a lower limit on density of neutrals (weaker than (2) and (3)).
7.	Adequate increase of electron temperature	Equation (30)	Sets a lower limit on amplitude of rf field.
8.	Assures validity of equation (17)	Equation (32)	Sets an upper limit on amplitude of rf field.
9.	Breakdown field not exceeded	———	Same as (8)
10.	Binary collision theory to be valid	———	Same as (8)
11.	Sufficient increase of electron temperature that radiation and reaction energy losses are small compared with other inelastic energy exchanges, but not so large that δ_{eff} changes much with increase in T_e	Equation (36)	Defines a permissible range for increase of electron temperature.

TABLE II

TYPICAL PLASMA TEMPERATURES IN ^{o}K FOR ARC HEATED PURE NITROGEN EXPANDED TO A PRESSURE OF APPROXIMATELY 400 MICRONS

T_o (a)	$T_{e, E=0}$ (b)	T_{vib} (c)	T_{rot} (d)	$T_{tr} = T_{static}$ (e)
1800	1720	1810	275	260
1950	1650	1880	295	290
2200	2800	2590	305	310
2400	2580	2660	320	350
2800	3230	2980	385	425
3050	3580	3450	420	475
3350	3620	3840	540	540

(a) Stagnation temperature from average enthalpy from arcjet energy balance.

(b) Electron temperature from Langmuir probe, electron beam off.

(c) Electron beam spectroscopy.

(d) Electron beam spectroscopy.

(e) From isentropic expansion.

TABLE III

TYPICAL ENERGY-LOSS FACTORS FOR ARGON AT A GAS TEMPERATURE BETWEEN 100 AND 200 ^{o}K

Electron Temp., $T_{e, E=0}$, ^{o}K	rf Power, watts	Electron Temp., T_e, ^{o}K (with rf)	Energy-loss Factor, δ_{eff}
3395	0.217	5660	3.00×10^{-5}
3220	0.220	5450	3.08×10^{-5}
2420	0.285	5330	3.06×10^{-5}
2165	0.2675	4655	3.35×10^{-5}
2150	0.275	4860	3.17×10^{-5}
2515	0.2975	5445	3.17×10^{-5}
2335	0.2965	5510	2.91×10^{-5}
2535	0.867	11320	3.08×10^{-5}
		Average:	3.10×10^{-5}

TABLE IV

TYPICAL ELECTRON TEMPERATURE MEASUREMENTS
AS A FUNCTION OF RF POWER FOR NITROGEN

RF Power:	0 watts	4.2 w	8.4 w	12.6 w	16.8 w
	Electron Temperature, ^{o}K				
	3500	4320			
	3490	4790			
	3390	4540			
		4590	5950		
		4640	5710		
			6110	7510	
	3540			7340	
	3410				8940
	3550				8680
Averages:	3480	4580	5920	7430	8810

TABLE V

TYPICAL ENERGY-LOSS FACTORS FOR NITROGEN
AS A FUNCTION OF GAS TEMPERATURE

Gas Temperature, ^{o}K $T_g = T^{+} = T_{e,E=0}$	rf Power, watts	Electron Temp., T_e, ^{o}K (with rf)	Energy-loss Factor, δ_{eff}
1260	2.32	3865	2.54×10^{-4}
1700	2.4	4130	2.9×10^{-4}
1715	2.24	3915	2.92×10^{-4}
1750 (Air leak)	4.2	3260	7.8×10^{-4}
2860	2.4	3950	6.3×10^{-4}
2940	2.4	3910	7.1×10^{-4}
3190	2.4	4315	6.1×10^{-4}
3190	0.8	3500	7.6×10^{-4}
3190	2.4	4250	6.5×10^{-4}
3480 (Air leak)	4.2	4580	10.9×10^{-4}
3610	2.4	4600	6.95×10^{-4}
3760	2.4	4790	6.7×10^{-4}
3830	2.24	4650	7.9×10^{-4}
3970	0.8	4320	6.5×10^{-4}
4280	2.4	5340	6.7×10^{-4}
5026	2.4	6065	6.6×10^{-4}
5950	2.4	6490	13.0×10^{-4}
6100	2.4	7540	4.9×10^{-4}

TABLE VI

TYPICAL ENERGY-LOSS FACTORS FOR OXYGEN-NITROGEN MIXTURES AS A FUNCTION OF COMPOSITION AND GAS AND ELECTRON TEMPERATURES ($R_Q = Q_{eN_2}/Q_{eO_2}$)

$\frac{[O_2]}{[O_2]+[N_2]}$	Gas temp. °K $T_g = T_{e,E=0}$	rf power W	Electron temp. T_e, °K (with rf)	Mixture energy-loss factor, $\delta_{eff} \times 10^4$	Derived energy loss factor for pure O_2, $\delta_{O_2} \times 10^4$, using $\delta_{N_2} = 3 \times 10^{-4}$ $R_Q = 2.5$	$R_Q = 2.0$
0	4060	2.4	4920	8.0		
0	3240	2.4	3950	9.7		
0	2960	4.8	4700	7.92		
0	3530	1.6	4280	6.12		
0.0356	2220	2.4	3210	6.96	274	221
0.0416	2030	2.4	3160	6.10	184	148
0.0453	1750	4.8	3415	8.27	286	230
0.0453	1815	8.0	3870	11.2	442	356
0.0834	2000	2.4	2550	12.5	274	222
0.0834	1730	4.8	2880	12.0	256	208
0.0834	1850	8.0	3360	15.2	346	284
0.1007	1630	4.8	2550	15.0	286	231
0.1251	1680	2.4	1920	28.7	476	389
0.1431	1850	8.0	2980	20.3	279	228
0.1666	1690	2.4	1970	24.6	294	241
0.1666	1865	8.0	2520	35.0	435	355

TABLE VI
(Concluded)

0.1850	1240	2.4	1580	20.3	211	173
0.2217	1680	8.0	2100	54.7	506	417
0.2217	1730	16.0	2440	64.7	606	498
0.2481	1660	2.4	1820	43.0	346	285
0.2481	1430	2.4	1700	25.5	196	162
0.3006	1440	2.4	1810	18.6	109	91
0.3211	1540	16.0	2520	46.9	279	233
0.3211	1630	28.0	2670	77.3	470	391
0.3333	1590	2.4	1750	43.0	243	203
0.4169	1495	2.4	1700	33.6	145	119
0.500	1275	16	2050	59.3	200	173
0.500	1760	56	4550	57.6	194	167
0.500	1595	2.4	1865	25.5	82	71
				Average:	297	244

TABLE VII

DEPENDENCE OF ENERGY LOSS FACTOR FOR PURE OXYGEN, DERIVED FROM MIXTURE DATA BY MIXTURE RULE[1] AND ASSUMING THAT ONLY N_2 AND O_2 ARE PRESENT IN THE MIXTURE, ON THE OXYGEN CONTENT OF THE MIXTURE ($R_Q = 2.5$)

$\frac{[O_2]}{[O_2] + [N_2]}$	Derived $\delta_{O_2} \times 10^4$
~0.04 (four runs)	296
0.083 (three runs)	292
~0.16 (four runs)	305
~0.23 (four runs)	413
~0.32 (four runs)	275
0.50 (three runs)	159

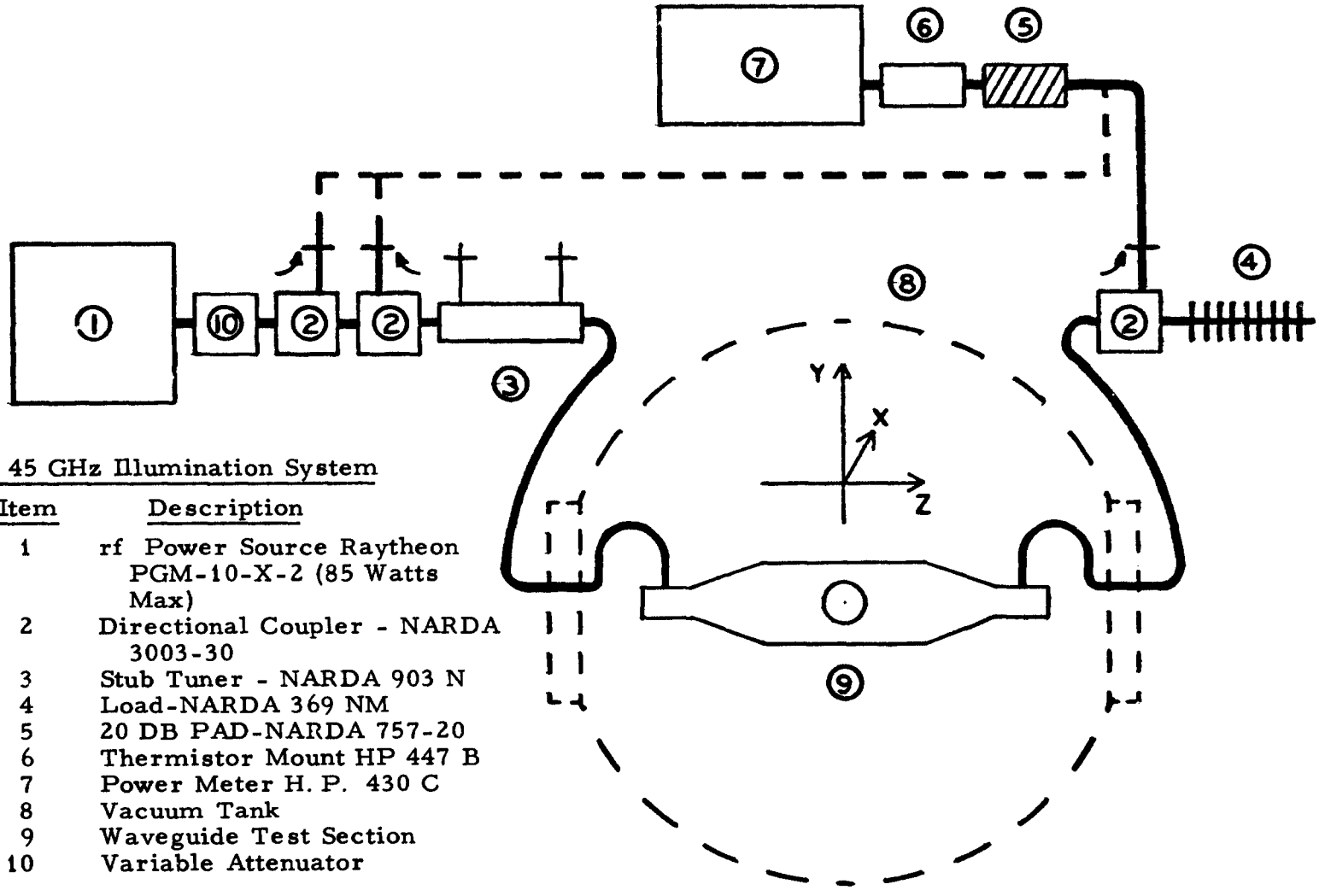

2.45 GHz Illumination System

Item	Description
1	rf Power Source Raytheon PGM-10-X-2 (85 Watts Max)
2	Directional Coupler - NARDA 3003-30
3	Stub Tuner - NARDA 903 N
4	Load-NARDA 369 NM
5	20 DB PAD-NARDA 757-20
6	Thermistor Mount HP 447 B
7	Power Meter H. P. 430 C
8	Vacuum Tank
9	Waveguide Test Section
10	Variable Attenuator

Figure 1. - Schematic of microwave plasma illumination system.

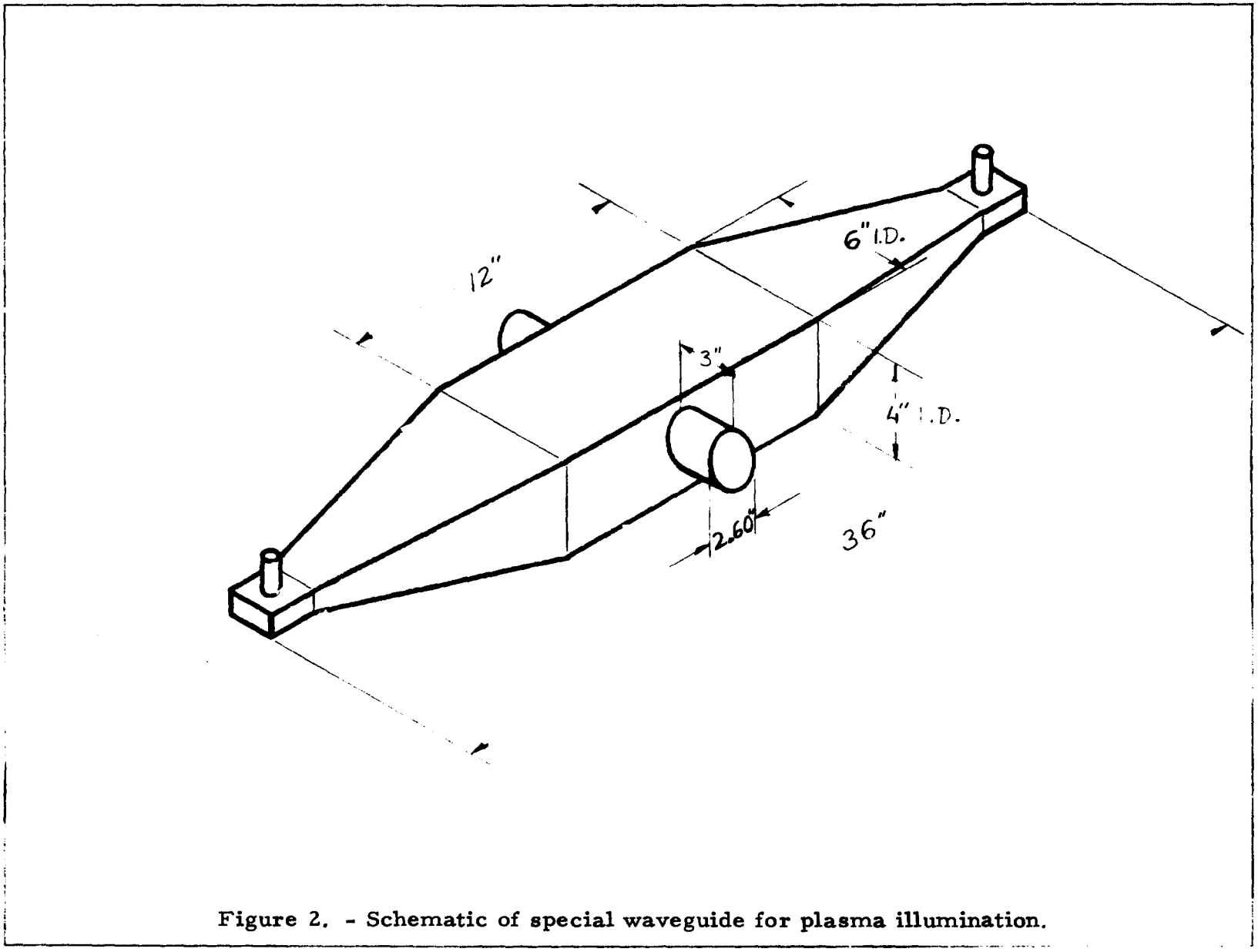

Figure 2. - Schematic of special waveguide for plasma illumination.

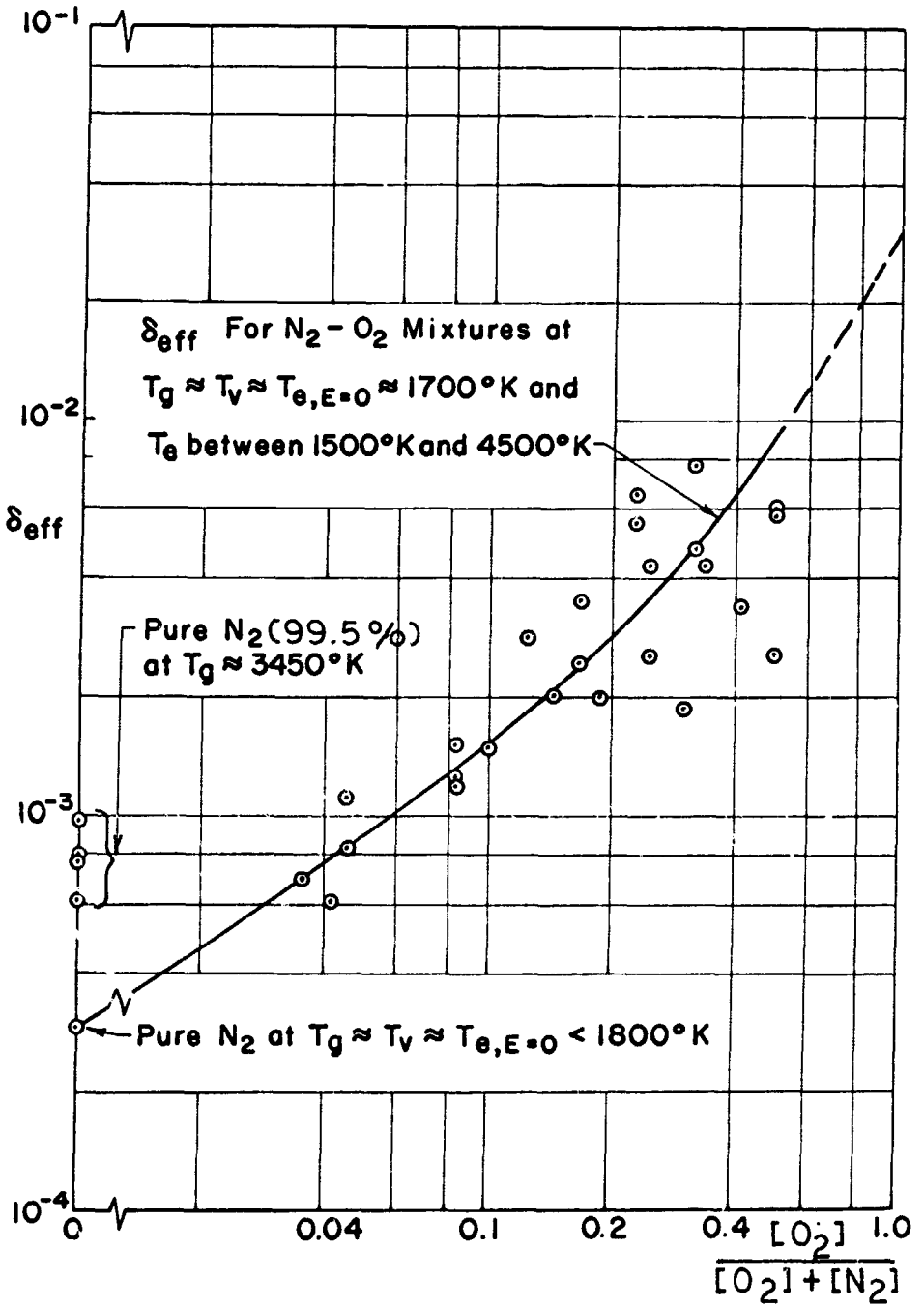

Figure 3. Energy-loss factor for N_2-O_2 mixtures at $T_g \approx T_{vib} \approx T_{e,E=0} \approx 1700\ ^{o}K$ as a function of oxygen mole fraction. Purity of N_2 is 99.5% as claimed by manufacturer.

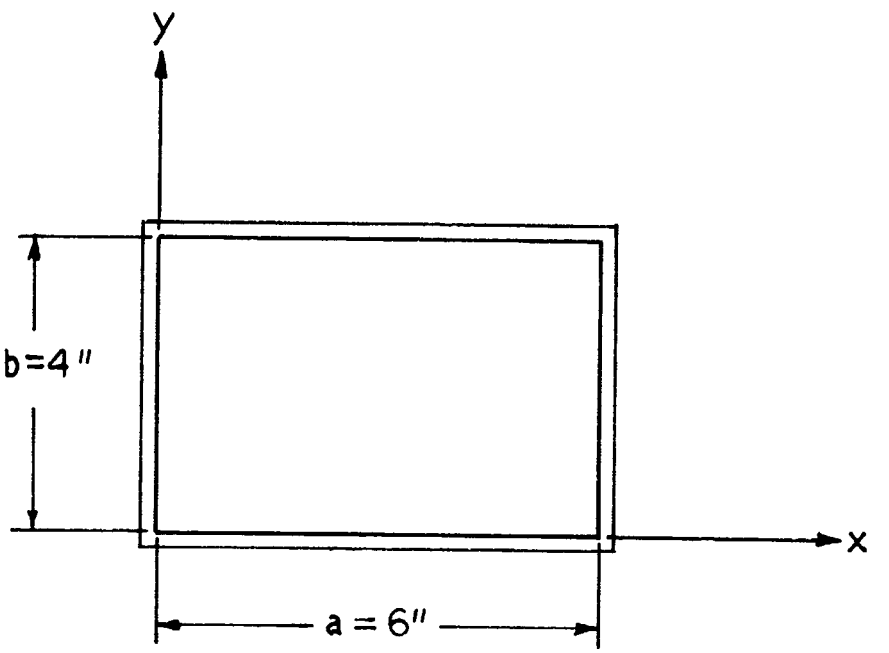

Figure 1A, Appendix A. Cross section of the waveguide. I. D.

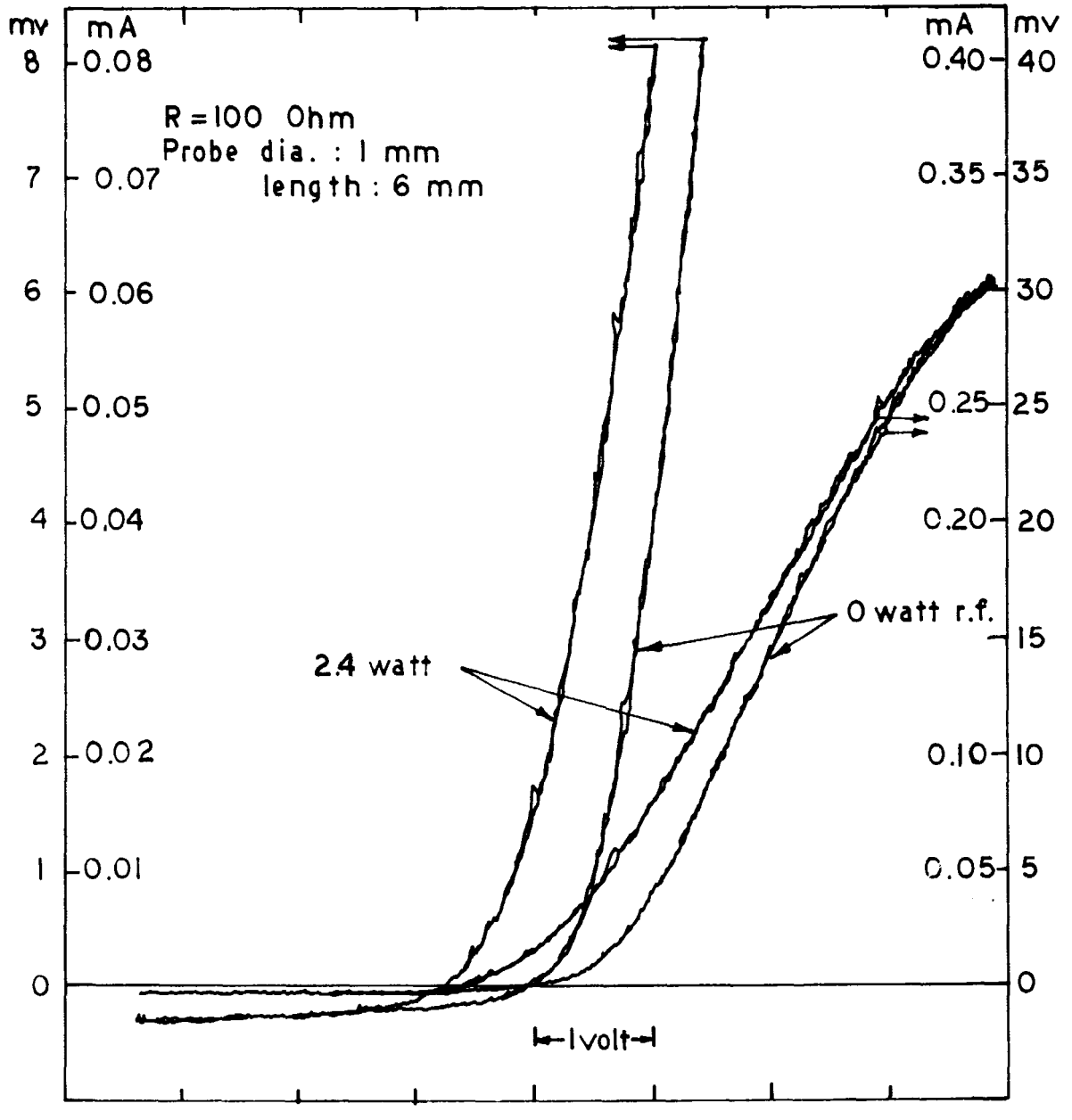

Figure 1, Appendix C. Langmuir probe characteristics for nitrogen plasmajet with 2.4 watts and 0 rf power (traced twice).

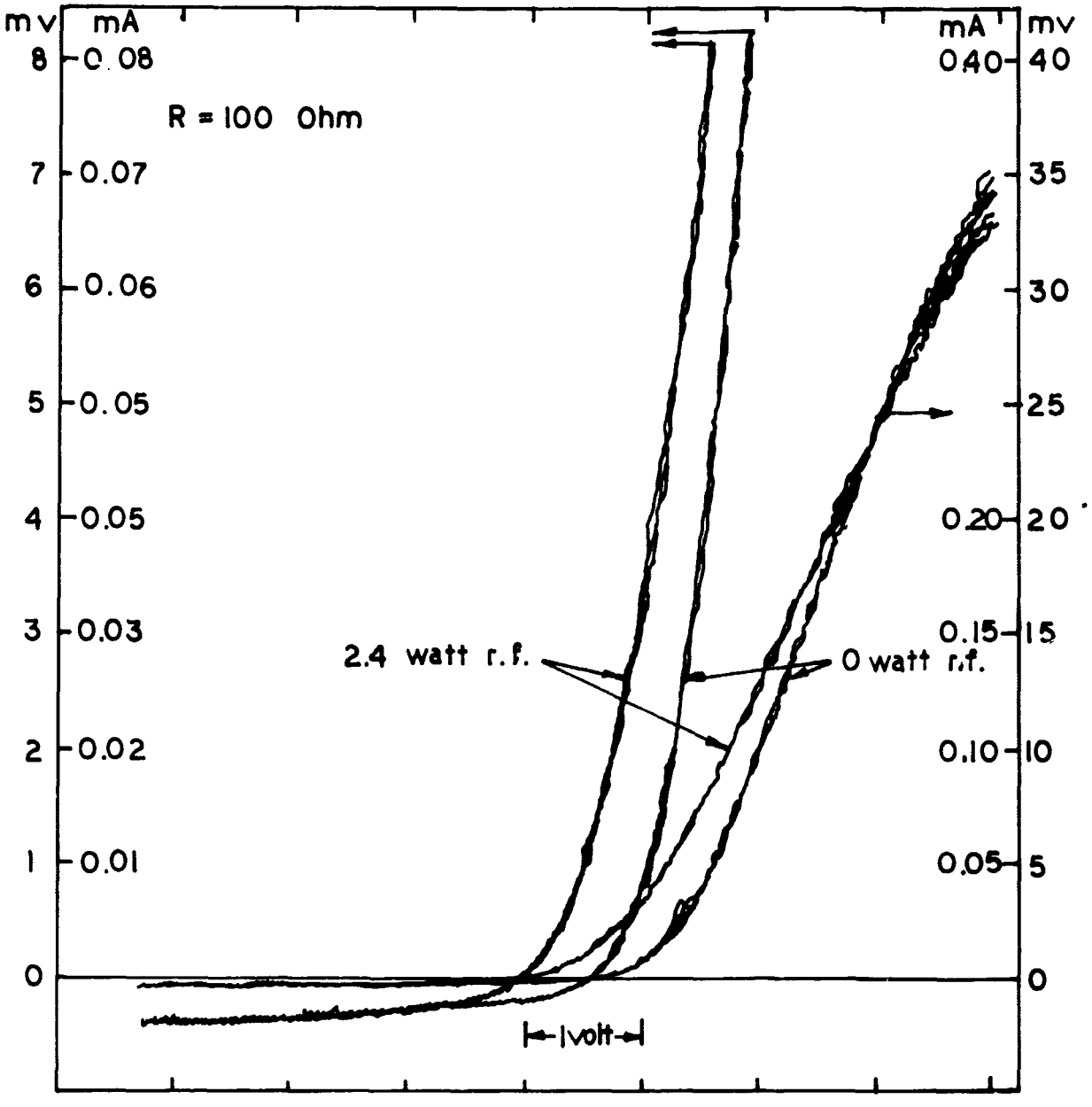

Figure 2, Appendix C. Langmuir probe characteristics for nitrogen plasmajet with 2.4 watts and 0 watts rf (traced five times).

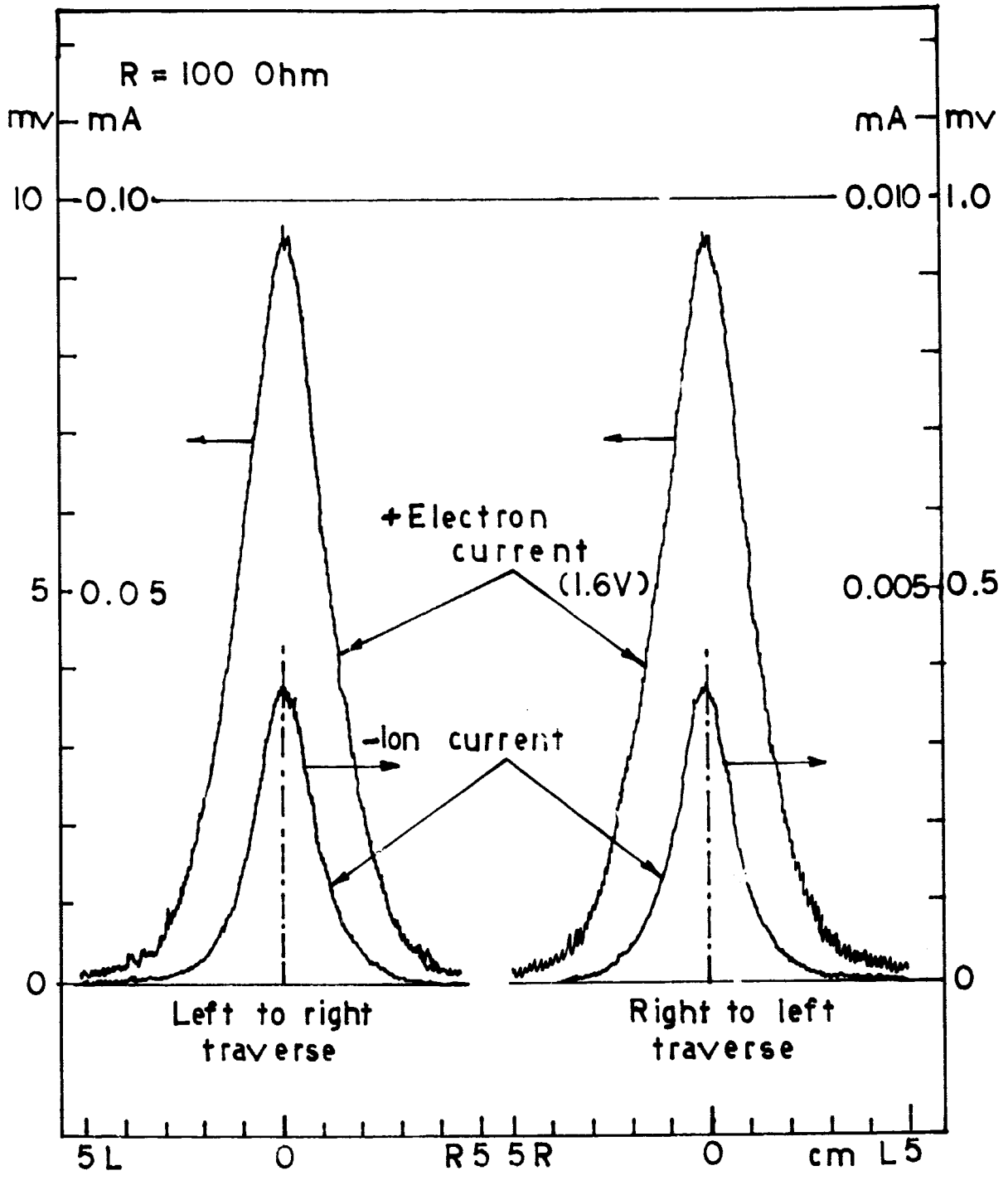

Figure 3, Appendix C. Radial survey of electron and ion current to Langmuir probe obtained by continuous traverses of probe through plasmajet axis.

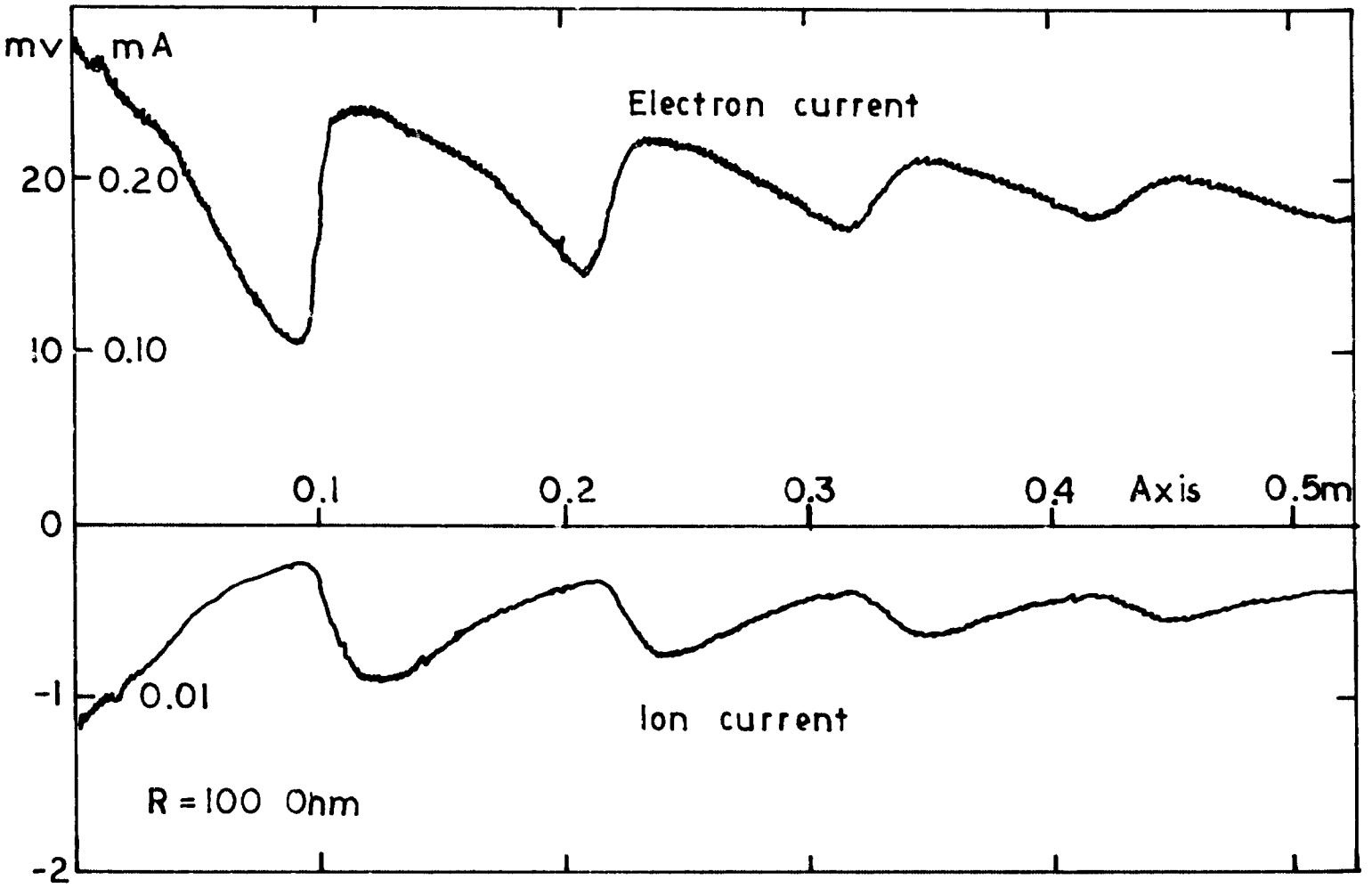

Figure 4, Appendix C. Axial survey of electron and ion current to Langmuir probe obtained by continuous traverses of probe along plasmajet axis. Peaks in electron current correspond to passage of probe through shock diamonds.

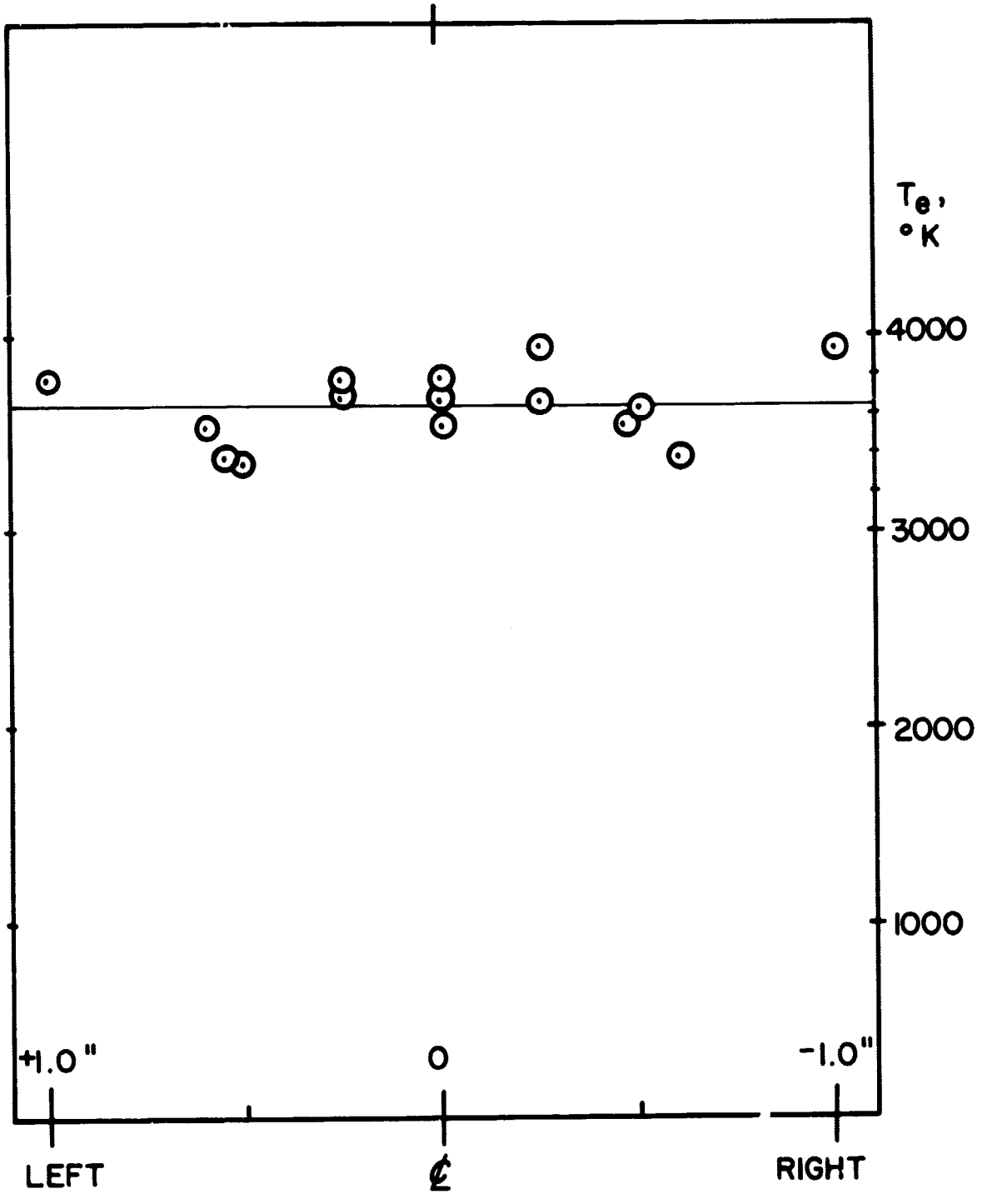

Figure 5, Appendix C. Radial distribution of T_e.

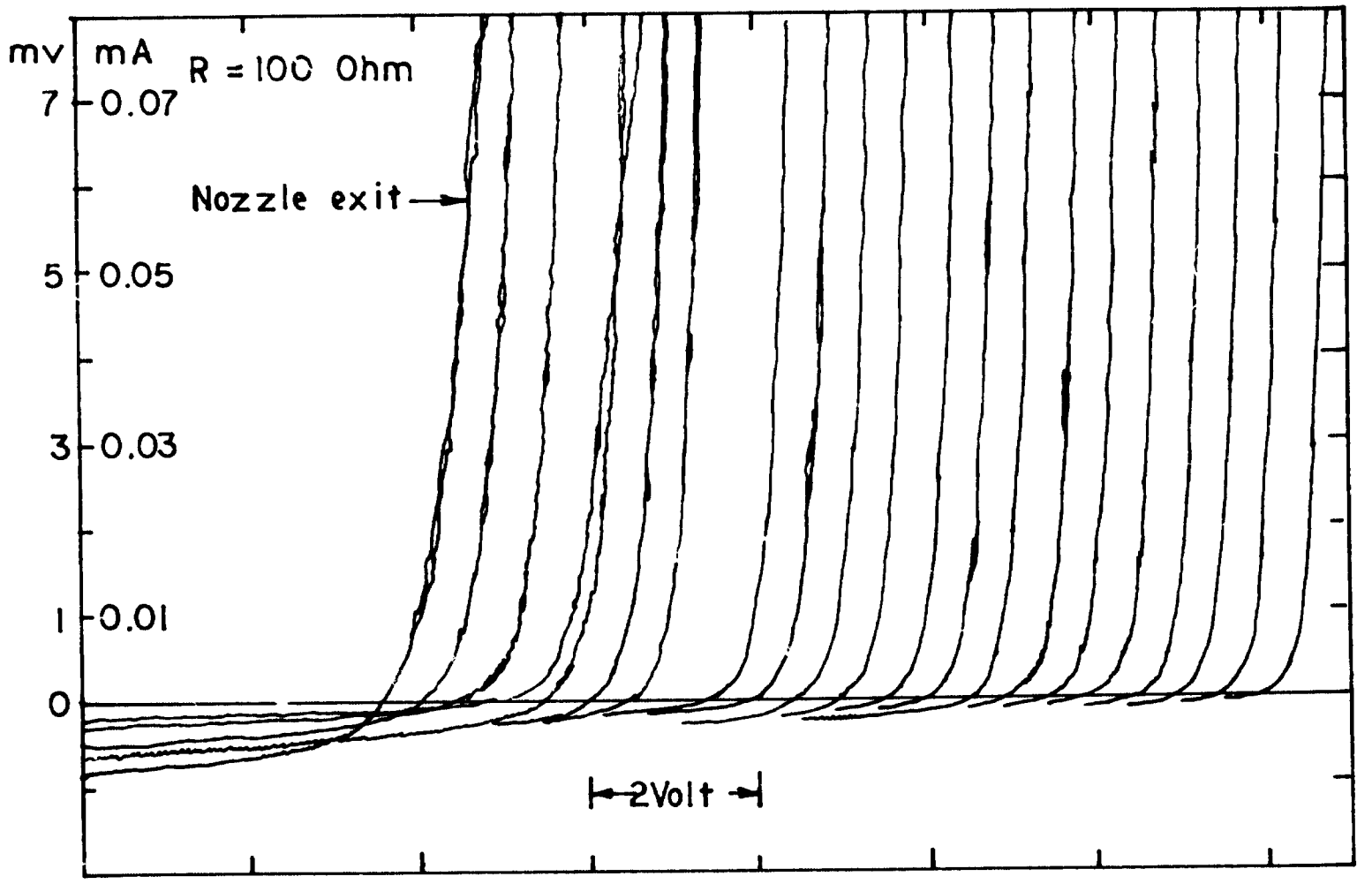

Figure 6, Appendix C. Langmuir probe characteristics along axis of plasmajet obtained at 1" intervals from nozzle exit to 20" downstream.

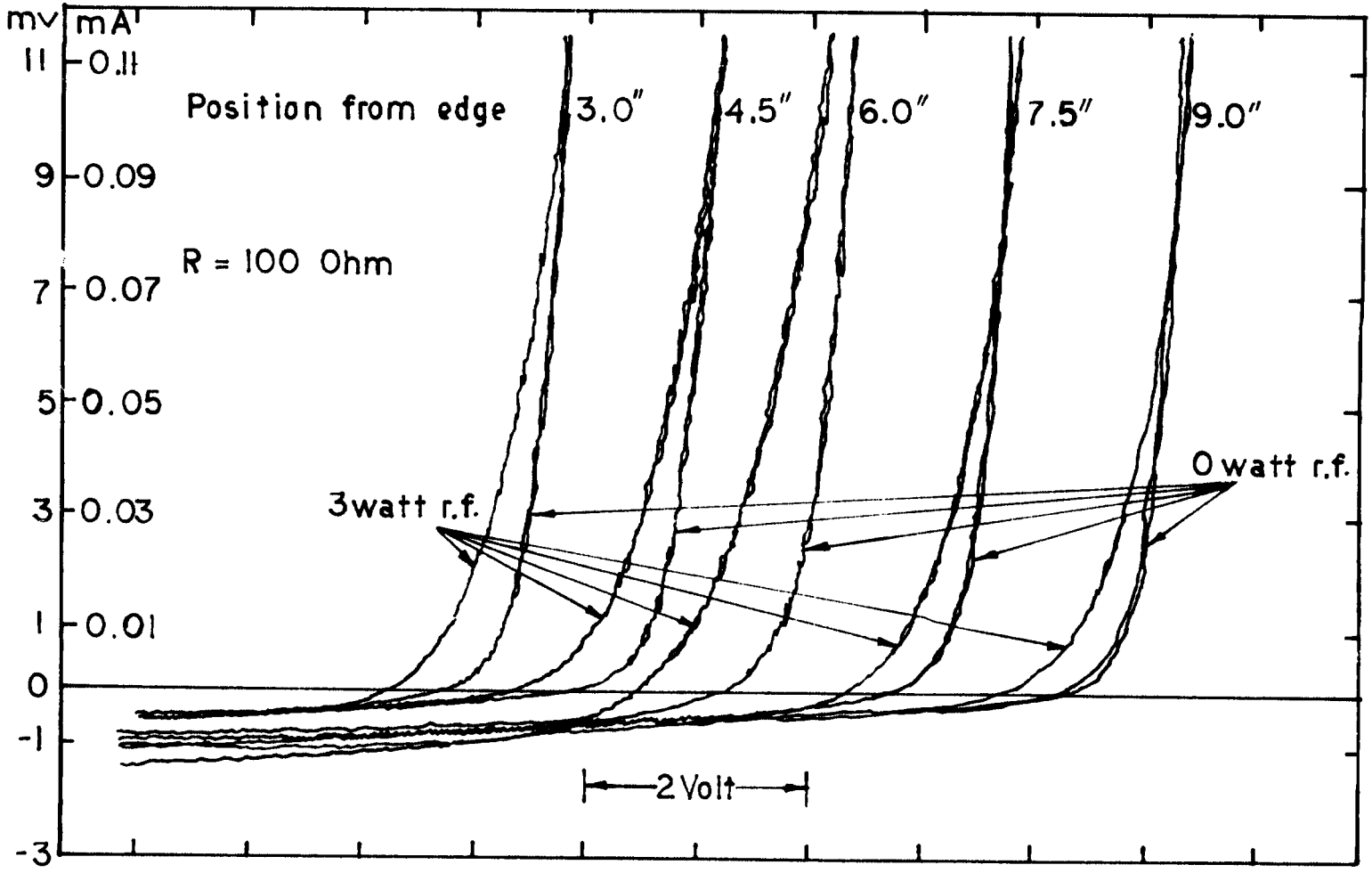

Figure 7. Appendix C. Langmuir probe characteristics along axis of jet inside cavity with 3 watt r.f. applied.

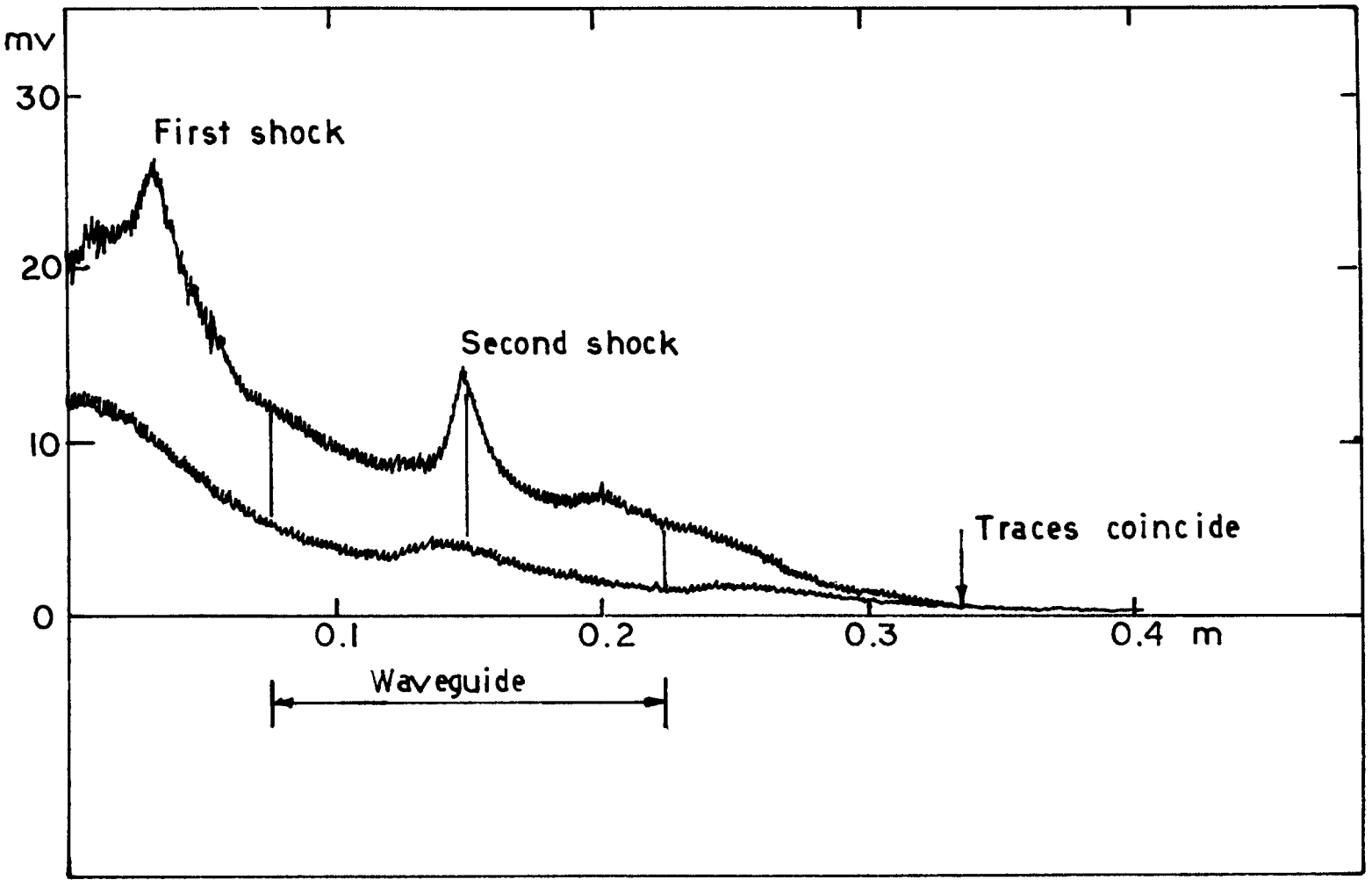

Figure 8, Appendix C. Effect of RF on probe electron current on jet axis (axial traverse). Note the effect is negligible outside waveguide (two traces come together).

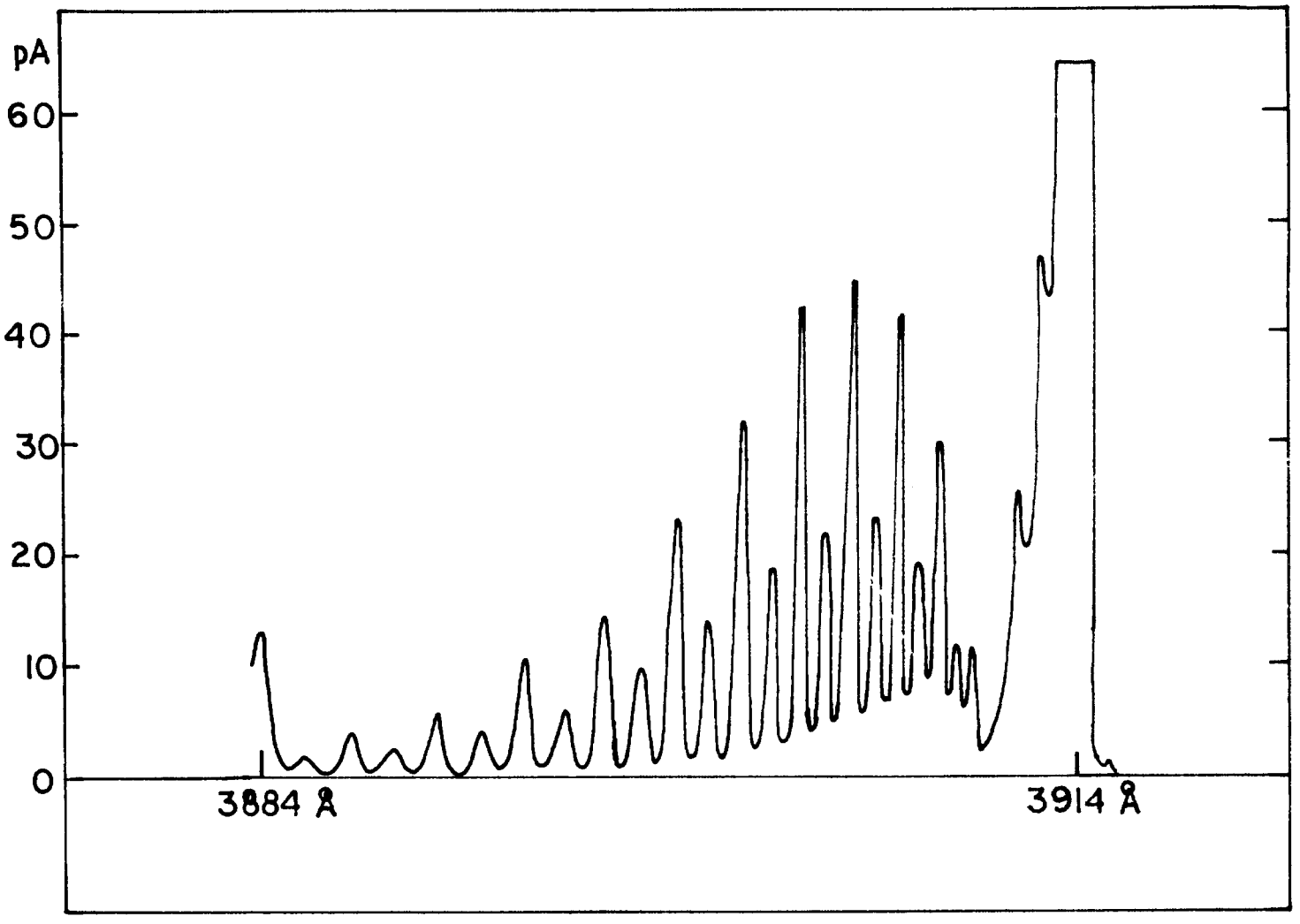

Figure 9, Appendix C. Rotational band of $N_2^+(0, 0)$ used to determine rotational temperature.

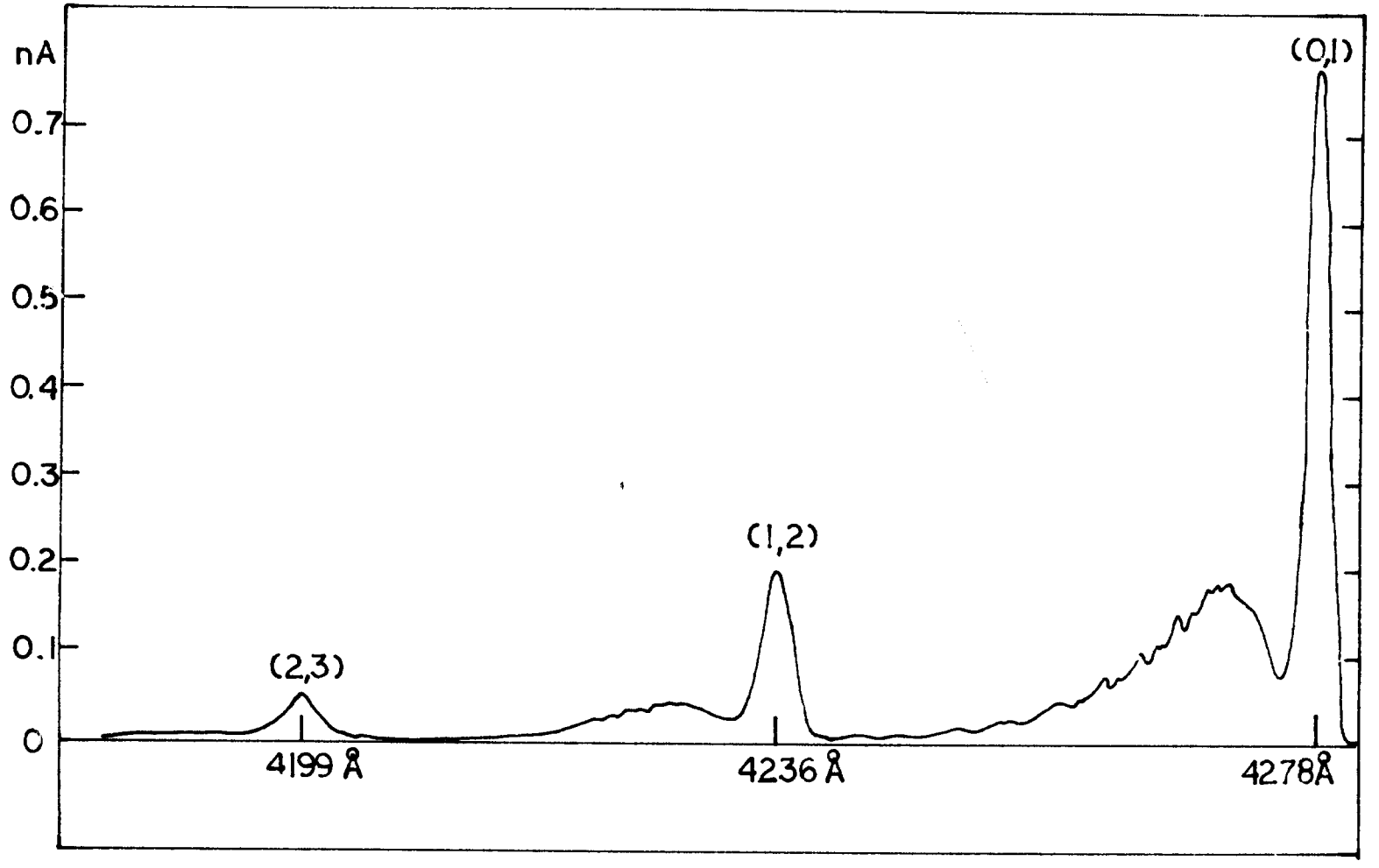

Figure 10, Appendix C. Band profiles of $N_2^+(0, 1)$ progression at $T_{vib} \approx 2000\ ^oK$, $T_{vib} \neq T_{rot}$ used to determine vibrational temperature.